J 9.2

MESOSCALE MODELING OF URBAN CIRCULATION FORCED BY AIRFLOW AND URBAN HEAT ISLAND

Albert. F. Kurbatskiy[1*] and Ludmila. I. Kurbatskaya[2]
[1]Institute of Theoretical and Applied Mechanics of Russian Academy of Sciences, Siberian Branch
[1]Department of Physics, Novosibirsk State University
Novosibirsk, Russia
[2]Institute of Computational Mathematics and Mathematical Geophysics SB RAS
Novosibirsk, Russia

1. INTRODUCTION

The complexity of problems on the quality of air in urbanized areas lies in the variety of spatiotemporal scales on which the processes of pollution dispersion and transformation proceed. In particular, two of the most important scales include an “urban scale” of a few tens of kilometers (typical size of a city), on which a primary emission of air pollution occurs, and a “mesoscale” of several hundred kilometers, on which secondary air pollutions are formed.

Therefore, the dispersion of pollutants depends strongly on both the structure of the urban boundary layer and its interactions with the boundary layer of the city’s environs and the synoptic flow. In order to determine the average and turbulent transport and chemical transformations of pollutants, it is necessary to accurately know major meteorological quantities such as wind; turbulent fluxes of momentum, heat, and mass; temperature; pressure; and humidity.

These quantities can be either interpolated from measurement data or obtained with numerical models. These models are bound to be capable of accurately describing the statistical characteristics of hydrothermodynamic fields on the urban scale and mesoscale.

The effects of urban roughness must be parameterized because the horizontal sizes of the region are on the order of the mesoscale (100 km) and the difference-grid spacing minimized with respect to computational-time consumption is generally within several hundred meters and, consequently, the structure of the urbanized surface of the city is difficult to resolve in details.

In review of Roth (2000), the two most important effects of an urbanized surface on the structure of air flow over it are indicated**:**

a) drag to the incident air flow from buildings (because of the difference of pressures across roughness elements) and

b) differential heating of urbanized surfaces, which is able to generate the so-called effect of an urban heat island.

A typical diagram of an urbanized surface (model of urban roughness) is presented in Fig. 1. The urban canopy layer, which is marked in the diagram as **1**, extends from the underlying surface to the top of buildings and is strongly influenced by the local characteristics. In this region, the local flow and the turbulence have a strong effect on the dispersion of pollutants. The urban boundary layer occupies the region extending from the urban canopy layer to the level at which the effect of the urbanized surface is no longer manifested (6). The urban boundary layer includes the layer of turbulent wake 3 (so-called inner boundary layer), which is influenced directly by roughness elements; the turbulent surface layer (2, 4); and the mixed layer (5). The urban boundary layer and the urban canopy layer are key elements in calculating the modification of the background winds (on the synoptic scale and mesoscale) by the city and in obtaining the local wind fields with high resolution.

The understanding of the required connection between these layers represents the principal complex problem of urban fluid mechanics (Fernando et al., 2001). Because of this problem and a number of other difficulties, the effect of urban roughness on the structure of the ABL turbulence in mesoscale models is usually considered in a simplified form via a specific parameterization scheme.

Models describing the turbulence to a different degree of completeness and different parameterizations of urban roughness have been used recently to simulate the processes of momentum and heat transfer and pollutant scattering in an urban boundary layer. The conventional $E - \varepsilon$ model of turbulence is employed by Vu et al.(2002) and the effect of stratification on turbulent momentum and heat transfer is taken into account through the methodology of Launder (1975), with introduction of corrections for stratification into the proportionality coefficient standing in the standard two-parameter expression for the turbulent viscosity. The shortcomings of this representation are universally known. The turbulent viscosity also depends on the mean-velocity gradient and vertical

* *Corresponding author address:* Albert F. Kurbatskiy, Inst. Theor. Appl. Mech. SB RAS, Novosibirsk State Univ., Dept. of Phys., 630090 Novosibirsk, Russia, e-mail: kurbat@nsu.ru

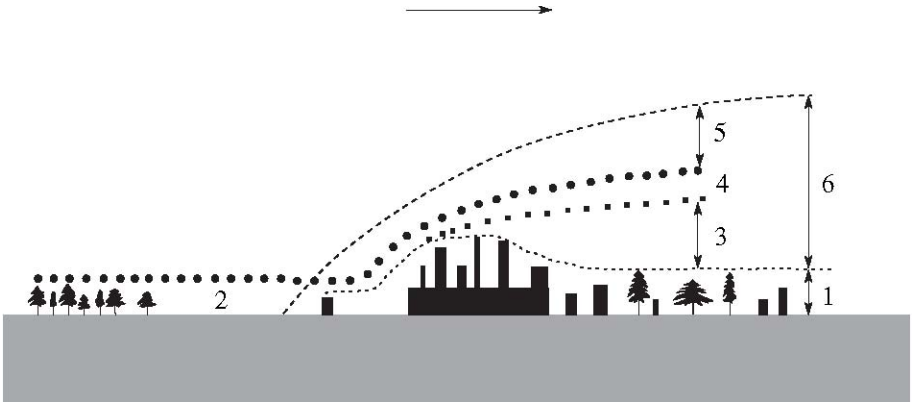

Figure 1. Typical urbanized area on a flat terrain.

turbulent heat flux (flux Richardson number) in addition to the turbulent kinetic energy *E* and its dissipation rate ε. Therefore, the turbulent momentum and heat fluxes are not expressed explicitly in terms of the mean-field gradients and an iteration procedure is required. To take into account the effect of roughness on heat-transfer processes and their influence on urban climate, the governing Navier–Stokes equations and the equation of heat inflow are averaged not only over an ensemble but also over space via introduction of a certain effective-volume function.

Another parameterization scheme of Martilli et al. (2002) uses the approximation of "porous urban roughness," in which the drag and frictional forces induced by buildings of different heights are taken into account in the form of source terms in the equations of motion and heat and moisture inflow via the method proposed of Raupach et al. (1991). A scheme of such a parameterization is depicted in Fig. 2b along with a horizontal-wind-velocity profile, which clearly shows the effect of urban roughness on flow in an urban canopy layer. A conventional rough-ness model and a profile of mean wind velocity are shown in Fig. 2a.

The two parameterization schemes are implemented in a simple two-dimensional test of ABL evolution through a one-parameter model of turbulence in which the turbulent kinetic energy alone is determined from the transport equation. For all turbulent fluxes, the gradient model of the K-theory with the linear turbulent scale regarded as a function of the vertical coordinate alone is used.

In this study, a scheme of parameterization of the roughness of the urbanized surface (Fig. 2b) is also implemented for a simple two-dimensional test. A modified three-parameter model of turbulence for the ABL over an urbanized surface with modeling of the effect of an urban heat island is used. Unlike the three-parameter model developed previously of Kurbatskii (2001), for the modified model, completely explicit anisotropic models are derived for the turbulent momentum fluxes (Reynolds stresses) and turbulent flux of the scalar via symbol algebra. The model provides additional possibilities for studying the effects of an inhomogeneous underlying surface (thermal and mechanical) on the pattern of a stratified atmospheric flow as compared to one- and two-parameter techniques of modeling the turbulence (see, for example, of Vu et al., 2002; Martilli et al.,2002).

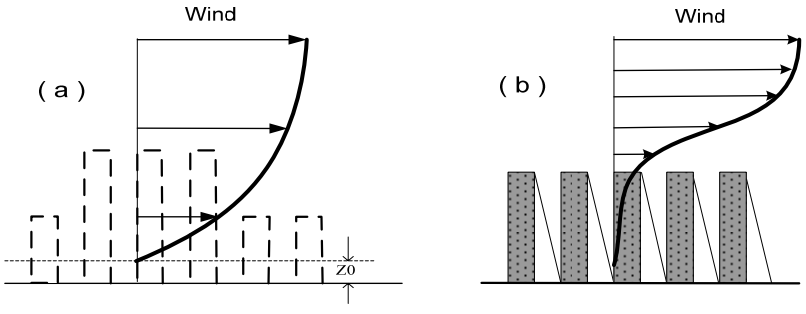

Figure 2. The concept of incorporation of urban canopy model**:** (a) –the conventional model, Z_0 - the roughness length; (b) – the urban canopy model.

Furthermore, Section 2 presents the governing equations and the basic relations of the modified three-parameter model for the turbulent ABL. In Section 3, the problem is formulated for a two-dimensional computational test, the initial and boundary conditions are stated, and the numerical method is briefly described. The results of the numerical test are described and analyzed in Section 4. In Section 5 comparison between $E-\varepsilon-\langle\theta^2\rangle$ and $k-\varepsilon$ turbulence models is resulted, and in Section 6 results of numerical modeling of passive tracer dispersion above city are presented. Brief conclusions are presented in Section 7. Finally, the Appendix (Section 8) presents the governing system of equations for a two-dimensional numerical test, completely explicit algebraic expressions for the turbulent momentum and heat fluxes, numerical values of the model's constants, the details of the scheme of parameterization of urban roughness, and boundary conditions.

2. MODIFIED THREE-PARAMETER MODEL FOR TURBULENT ATMOSPHERIC BOUNDARY LAYER

Studies of the parameterization of turbulence were started in the 1940s according to Kolmogorov (1942). Models for turbulent stresses were subsequently verified experimentally on the basis of measurement data and from comparison with data obtained through large-eddy simulation and were applied in different engineering flows. In geophysical applications, turbulence closure models of different levels of complexity were formulated of Mellor and Yamada (1974, 1982; hereafter MY model) and were used to simulate a planetary boundary model more successfully than many other empirical models.

An improved turbulence closure model of level 2.5 was used by Cheng et al. (2002) for a planetary boundary layer. In this model, some simplifications of the original MY model were eliminated via the most complete models developed by Zeman and Lumley (1979) for the pressure-velocity Π_{ij} and pressure-temperature correlation Π_i^θ (see below equations. 2a and 3a). In the turbulence model of level 2.5, all turbulent fluxes of momentum (Reynolds stresses) and turbulent fluxes of heat, including the temperature variance $\langle\theta^2\rangle$, are determined from algebraic expressions.

Launder et al. (1975) and Launder (1996) somewhat different (but also tensor-invariant, as well as at Zeman and Lumley, 1979) models are proposed for the correlations of Π_{ij} and Π_i^θ. These models are used in this study in formulating the three-parameter model of turbulence. Following of Zeman and Lumley (1979), the parameterizations of the correlations of Π_{ij} and Π_i^θ of Cheng et al. (2002) include buoyancy effects, whereas the tensor-invariant IP model of Launder (1996) is used for the rapid terms of these correlations, $\Pi_{ij}^{(2)}$ and $\Pi_i^{(\theta 2)}$ (see below the expressions of (7b)). The rapid parts of both Π_{ij} and Π_i^θ contain velocity terms related to the mean strain-rate tensor S_{ij}, and the vorticity tensor R_{ij}, as well as buoyancy terms related to the heat fluxes. The model for the slow part of the pressure-velocity correlation has a simple relaxation form: $\Pi_{ij}^{(1)} = -b_{ij}/\tau$, where $b_{ij} = \langle u_i u_j\rangle - (2E/3)\delta_{ij}$ is the anisotropy tensor, $E = \langle u_i u_i\rangle/2$ is the turbulent kinetic energy (TKE), $\tau = E/\varepsilon$ is the return-to-isotropy time scale, and ε is the TKE dissipation. The tensor S_{ij} and R_{ij} in the rapid part of correlation $\Pi_{ij}^{(2)}$ have the same numerical coefficients as well as Launder (1975, 1996) and different coefficients in the models of Zeman and Lumley (1979) and Cheng et al. (2002). The original closure MY model of level 2.5 is based on simpler parameterizations for the pressure-velocity and pressure-temperature correlations: $\Pi_{ij}^{(1)} \approx b_{ij}/\tau$, $\Pi_{ij}^{(2)} \approx ES_{ij}$, and $\Pi_{ij}^{(3)} = 0$ (buoyancy contribution); $\Pi_i^{(\theta 1)} \approx h_i/\tau_\theta$, where $h_i = \langle u_i\theta\rangle$ is the vector of turbulent heat flux and τ_θ is the time scale of the turbulent temperature field, and $\Pi_i^{(\theta 2)} = \Pi_i^{(\theta 3)} = 0$. Consequently, the MY model takes into account one rapid term ($\Pi_{ij}^{(2)}$) and disregards the effects of buoyancy (the terms $\Pi_i^{(\theta 2)}$, $\Pi_i^{(\theta 3)}$).

Thus, the parameterizations used in this study for the turbulent momentum and heat fluxes are intermediate between the parameterizations of the improved model of Cheng et al. (2002) and those of the MY model. The improved closure model of level 2.5 was subject to testing by Cheng et al. (2002) during the solution of the standard problem of a horizontally homogeneous planetary boundary layer. However, even for this simple problem, an accurate calculation of the countergradient heat flux in the inversion layer is required under conditions of unstable stratification. In this case, an algebraic parameterization, which is used in models of level 2.5, is insufficient to calculate the temperature variance $\langle\theta^2\rangle$ and the solution of the transport equation for the variance of temperature is needed to correctly take into account the processes of advection, diffusion, and destruction for this quantity.

2.1 *Governing Equations*

Equations for the mean and turbulent quantities are necessary to model flows in the atmospheric boundary layer. The governing equations the mean velocity U_i and mean potential temperature Θ may be written as

$$\frac{DU_i}{Dt} = -\frac{\partial \tau_{ij}}{\partial x_j} - g_i - \frac{1}{\rho}\frac{\partial P}{\partial x_i} - 2\varepsilon_{ijk}\Omega_j U_k + \hat{D}_{u_i} \quad (1a)$$

and

$$\frac{D\Theta}{Dt} = -\frac{\partial}{\partial x_j} h_j + \hat{D}_\theta, \quad (1b)$$

respectively. Here,

$$\frac{D}{Dt} \equiv \frac{\partial}{\partial t} + U_j \frac{\partial}{\partial x_j}, \quad \tau_{ij} \equiv \langle u_i u_j \rangle, \quad h_i \equiv \langle u_i \theta \rangle, \quad (1c)$$

$\hat{D}_{u_i}$ is the source of forces (friction, form drag) induced by interactions between rigid surfaces (ground, buildings) and the air flow, $\hat{D}_\theta$ takes into account the effect of sensible heat fluxes from the rigid surfaces on the potential-temperature balance, u_i is a component of the turbulent velocity fluctuation, $g_i = (0, 0, g)$ is the vector of gravitational acceleration, P is the mean pressure, ρ is the mean density, Ω_j is the angular velocity of the Earth's rotation, τ_{ij} is the Reynolds stresses, and h_i is the vector of turbulent heat flux.

2.2 *Equations of Turbulence*

(i) Equations for the Reynolds stresses $\tau_{ij} \equiv \langle u_i u_j \rangle$

$$\frac{D}{Dt}\tau_{ij} + D_{ij} = -\left(\tau_{ik}\frac{\partial U_j}{\partial x_k} + \tau_{jk}\frac{\partial U_i}{\partial x_k}\right) + \beta_i h_j + \beta_j h_i - \Pi_{ij} - \varepsilon_{ij}, \quad (2a)$$

where

$$\Pi_{ij} \equiv \left\langle u_i \frac{\partial p}{\partial x_j} \right\rangle + \left\langle u_j \frac{\partial p}{\partial x_i} \right\rangle - \frac{2}{3}\delta_{ij}\frac{\partial}{\partial x_k}\langle p u_k \rangle, \quad (2b)$$

$$\varepsilon_{ij} \equiv 2\nu \left\langle \frac{\partial u_i}{\partial x_k}\frac{\partial u_j}{\partial x_k} \right\rangle = \frac{2}{3}\delta_{ij}\varepsilon, \quad \beta_i \equiv \beta g_i, \quad (2c)$$

$$D_{ij} \equiv \frac{\partial}{\partial x_k}\left(\langle u_i u_j u_k \rangle + \frac{2}{3}\delta_{ij}\langle p u_k \rangle \right). \quad (2d)$$

Here, Π_{ij} is the tensor of pressure–strain correlation, D_{ij} is the diffusion term, ν is the coefficient of molecular viscosity, β is the volumetric expansion rate of air, and p is the turbulent pressure fluctuation.

(ii) TKE balance equation

$$\frac{DE}{Dt} + \frac{1}{2}D_{ii} = -\tau_{ij}\frac{\partial U_i}{\partial x_j} + \beta_i h_i - \varepsilon + \hat{D}_E, \quad (2e)$$

where $\hat{D}_E$ is the source of the TKE generated because of interactions between buildings in the urban canopy layer and the air flow.

(iii) Transport equation for the turbulent heat flux $h_i \equiv \langle u_i \theta \rangle$

$$\frac{D}{Dt}h_i + D_i^h = -h_j\frac{\partial U_i}{\partial x_j} - \tau_{ij}\frac{\partial \Theta}{\partial x_j} + \beta_i\langle \theta^2 \rangle - \Pi_i^\theta, \quad (3a)$$

where $\Pi_i^\theta \equiv \left\langle \theta \frac{\partial p}{\partial x_i} \right\rangle$, $D_i^h = \frac{\partial}{\partial x_j}\langle u_i u_j \theta \rangle$, (3b)

Π_i^θ is the pressure–temperature correlation, and D_i^h is the diffusion of the heat flux h_i.

(iv) Transport equation for the variance of temperature $\langle \theta^2 \rangle$

$$\frac{D}{Dt}\langle \theta^2 \rangle + D_\theta = -2h_i\frac{\partial \Theta}{\partial x_i} - 2\varepsilon_\theta, \quad (4a)$$

$$\varepsilon_\theta \equiv \chi\left\langle \left(\frac{\partial \theta}{\partial x_j}\right)^2 \right\rangle, \quad D_\theta = \frac{\partial}{\partial x_i}\langle u_i \theta^2 \rangle, \quad (4b)$$

where χ is the molecular thermal diffusivity, D_θ is the diffusion of the variance of temperature, and ε_θ is the dissipation rate of the variance of temperature.

(v) Equation of TKE spectral consumption (TKE dissipation rate)

$$\frac{D\varepsilon}{Dt} + D_\varepsilon = -\frac{\varepsilon}{\tau}\Psi + \hat{D}_\varepsilon, \quad (5a)$$

where

$$\Psi = \psi_0 + \psi_1\frac{b_{ij}}{\varepsilon}\frac{\partial U_i}{\partial x_j} + \psi_2\frac{\beta_i}{\varepsilon}\langle \theta u_i \rangle + \psi_3\beta_j\frac{2E}{\varepsilon}\langle \theta u_i \rangle\frac{\partial U_i}{\partial x_j} \quad (5b)$$

$$D_\varepsilon = \frac{\partial}{\partial x_j}\langle \varepsilon u_j \rangle, \quad (5c)$$

and $\hat{D}_\varepsilon$ is the source of "secondary" dissipation,

and $\hat{D}_\varepsilon$ is the source of "secondary" dissipation, which is due to the presence of buildings in the urban canopy layer. The interaction of the buildings with the air flow leads to an increase in the cascade of energy

from the mean kinetic energy to the TKE and, consequently, to an increase in dissipation.

In this study, the terms containing the molecular viscosity ν and thermal diffusivity χ are disregarded everywhere except in the expressions for ε_{ij} and ε_θ. Moreover, rotation is also disregarded in the equations for second moments. Modeling the third-order moments is beyond the scope of this study. As noted above, the main problem was to obtain parameterizations for the turbulent momentum and heat fluxes in the approximation of weakly equilibrium turbulence (Girimaji and Balachandar, 1998), which does not require the modeling of the third-order moments.

The approximation of weakly equilibrium turbulence is based on the assumption that, in slowly evolving turbulent flows, the means of velocity, temperature, and other hydrothermodynamic fields vary in space and time more slowly than turbulent quantities (turbulent stresses, turbulent fluxes of a scalar, variances) and, consequently, the turbulence is approximately in equilibrium with the imposed mean fields. In this equilibrium state, the material derivatives of the anisotropy tensor of stresses b_{ij} and the vector of turbulent scalar (temperature) flux are approximately equal to zero: the turbulence reaches an equilibrium state, in which the equilibrium values of the tensor b_{ij} and vector h_i are independent of the initial conditions

2.3 *Turbulence Closure: Models for Pressure – Strain and Pressure –Scalar Correlations*

Three-parameter model of thermally stratified turbulence. As compared to the conventional method of modeling a planetary boundary layer, when a parameterization of the form $\varepsilon \sim E^{3/2}/\Lambda$ (Λ is the linear size of energy-containing turbulent eddies) is used for the TKE dissipation rate, it is preferable to employ another more universal and widely used approach in which the quantity ε is found from the solution of the differential transport equation (5a). Here, this equation is used in the same form given by (Kurbatskii, 2001; Kurbatskii and Kurbatskaya, 2001) and with the same numerical coefficients the values of which have been calibrated by different authors (see, for example, Kurbatskii, 2001; Sommer and So, 1995; Andren, 1990) and the values of the numerical coefficients ψ_0, ψ_1, ψ_2, and ψ_3 are given in the Appendix.

The transport equation for the destruction of temperature fluctuations ε_θ is more difficult to calibrate than the equation for the TKE dissipation. Instead of this equation, we use the parameterization

$$\varepsilon_\theta = \frac{\langle \theta^2 \rangle}{\tau_\theta}, \tag{6a}$$

where the time scale of the temperature field τ_θ is calculated from the ratio of the time scales of the temperature and dynamic fields

$$R = \frac{\tau_\theta}{\tau} = \frac{\langle \theta^2 \rangle}{2\varepsilon_\theta}\frac{\varepsilon}{E} \tag{6b}$$

The assumption of the constancy of this ratio yields reasonably accurate results for both engineering (Kurbatskii and Kazakov, 1999) and geophysical (Kurbatskii, 2001; Kurbatskii and Kurbatskaya, 2001) flows at $R = 0.6$.

For the diffusion terms D_{ii}, D_θ and D_ε, the following simple gradient-diffusion approximations are used (Kurbatskii and Kurbatskaya, 2001):

$$\frac{1}{2}D_{ii} = -\frac{\partial}{\partial x_i}\left(\frac{c_\mu}{\sigma_E}\frac{E^2}{\varepsilon}\frac{\partial E}{\partial x_i}\right), \tag{6c}$$

$$D_\varepsilon = -\frac{\partial}{\partial x_i}\left(\frac{c_\mu}{\sigma_\varepsilon}\frac{E^2}{\varepsilon}\frac{\partial \varepsilon}{\partial x_i}\right), \tag{6d}$$

$$D_\theta = -\frac{\partial}{\partial x_i}\left(\frac{c_\mu}{\sigma_\theta}\frac{E^2}{\varepsilon}\frac{\partial \langle \theta^2 \rangle}{\partial x_i}\right), \tag{6e}$$

where c_μ= 0.09 (Kurbatskii and Kurbatskaya, 2001).

The closed-form equations given in (2e), (4a), and (5a) form a three-parameter model of a thermally stratified turbulence.

Models of correlations with pressure fluctuations.

The pressure-velocity Π_{ij} and pressure-temperature Π_i^θ correlations in Eqs. (2a) and (3a) contain three different contributions caused by (i) self-interactions of the turbulence field (tending to isotropy or a slow part of correlation), (ii) interactions between the mean velocity shear and the turbulence (a rapid part of correlation), and (iii) interactions between the buoyancy and the turbulence (a rapid part of correlation as well):

$$\begin{aligned} &\Pi_{ij} = \Pi_{ij}^{(1)} + \Pi_{ij}^{(2)} + \Pi_{ij}^{(3)} \\ &\Pi_i^\theta = \Pi_i^{(\theta 1)} + \Pi_i^{(\theta 2)} + \Pi_i^{(\theta 3)} \end{aligned} \tag{7a}$$

$$\Pi_{ij}^{(1)} = c_1 \tau^{-1} b_{ij};$$

$$\Pi_{ij}^{(2)} = -(4/3)c_2 E S_{ij} - c_2(Z_{ij} + \Sigma_{ij}),$$

$$\Pi_{ij}^{(3)} = c_3 B_{ij},$$

$$\Pi_i^{(\theta 1)} = c_{1\theta}\tau^{-1}h_i,\ \Pi_i^{(\theta 2)} = -c_{2\theta}h_j\frac{\partial U_i}{\partial x_j},$$

$$\Pi_i^{(\theta 3)} = c_{3\theta}\beta_i\langle\theta^2\rangle\,, \tag{7b}$$

where

$$S_{ij} = \frac{1}{2}\left(\frac{\partial U_i}{\partial x_j} + \frac{\partial U_j}{\partial x_i}\right),\ R_{ij} = \frac{1}{2}\left(\frac{\partial U_i}{\partial x_j} - \frac{\partial U_j}{\partial x_i}\right); \tag{7c}$$

$$\Sigma_{ij} = b_{ik}S_{kj} + S_{ik}b_{kj} - \frac{2}{3}\delta_{ij}b_{km}S_{mk}\,,\ Z_{ij} = R_{ik}b_{kj} - b_{ik}R_{kj}\,,$$

$$B_{ij} = \beta_i h_j + \beta_j h_i - \frac{2}{3}\delta_{ij}\beta_k h_k \tag{7d}$$

Here, S_{ij} and R_{ij} are the tensors of mean shear and mean vorticity, respectively. As mentioned above, the tensor-invariant IP model (Launder et al., 1975; Launder, 1996) is used for a rapid part of correlation $\Pi_{ij}^{(2)}$.

Algebraic models of the Reynolds stresses and vector of heat flux. The combination of Eqs. (2a) and (2e) makes it possible to write the equation for the anisotropy tensor b_{ij} in the form

$$\frac{D}{Dt}b_{ij} + D_{ij} = -\frac{4}{3}ES_{ij} - \Sigma_{ij} - Z_{ij} + B_{ij} - \Pi_{ij}\,, \tag{8a}$$

where

$$D_{ij} \equiv \frac{\partial}{\partial x_k}\left\langle\left(u_i u_j - \frac{1}{3}u_l u_l\delta_{ij}\right)u_k\right\rangle. \tag{8b}$$

Equation (8a) can be simplified in the approximation of the weak equilibrium turbulence, where it is usually assumed that the diffusion term described by the tensor D_{ij} according to (8b) is also small. The substitution of expression (7b) for the pressure–strain correlation Π_{ij} into the right-hand side of Eq. (8a) leads to the following algebraic equation for the anisotropy tensor of turbulent stresses b_{ij}:

$$b_{ij} = -\alpha_1 E\tau S_{ij} - \alpha_2\tau\left(\Sigma_{ij} + Z_{ij}\right) + \alpha_3\tau B_{ij}\,, \tag{9a}$$

$$\alpha_1 = \frac{4}{3}\frac{1-c_2}{c_1},\ \alpha_2 = \frac{1-c_2}{c_1},\ \alpha_3 = \frac{1-c_3}{c_1}. \tag{9b}$$

Applying the approximation of weakly equilibrium turbulence to prognostic equation (3a) and using expression (7b) for the correlation Π_i^{θ}, we obtain the following algebraic equation for the vector of heat flux $\mathrm{h_i}$ at closure level 3.0 (according to the terminology of Mellor and Yamada 1974, 1982):

$$A_{ij}h_j = -\tau\left(b_{ij} + \frac{2}{3}E\delta_{ij}\right)\frac{\partial\Theta}{\partial x_j} + \tau\alpha_4\beta g\delta_{i3}\left\langle\theta^2\right\rangle, \tag{10a}$$

$$A_{ij} = c_{1\theta}\delta_{ij} + \tau\alpha_4\frac{\partial U_i}{\partial x_j} \tag{10b}$$

$$\alpha_4 = (1 - c_{2\theta})\,. \tag{10c}$$

We note that, for thermally stratified turbulence, the variance of temperature fluctuation $\langle\theta^2\rangle$ in the model of level 3.0 is not parameterized but obtained from the prognostic differential transport equation given in (4a). Thus, algebraic expressions for the turbulent momentum and heat fluxes assume a closed form when the three-parameter $E - \varepsilon - \langle\theta^2\rangle$ model of turbulence is used.

Explicit algebraic expressions for the turbulent momentum and heat fluxes and numerical values of the model's constants c_1, c_2, c_3, $c_{1\theta}$, and $c_{2\theta}$ are given in the Appendix.

Parameterization of urban roughness. As noted in the Introduction, the parameterization of urban roughness is performed in this study according to the scheme shown in Fig. 2b, which takes into account buildings of different height. Specific expressions used to calculate (in the governing equations) the effects of urban roughness on flow in the ABL are presented in the Appendix.

3. COMPUTATIONAL TEST

The three-parameter model of turbulence formulated above is used to study the effect of urbanized-surface roughness and an urban heat island on a global structure of the ABL during its 24-h cycle of evolution in a simple two-dimensional test.

3.1. *Computational Procedure: Initial and Boundary Conditions*

The horizontal extent of the integration domain is 120 km with a resolution of 1 km. The vertical resolution is 10 m within the first 50 m from the underlying surface, with the subsequent stretching of the grid in the vertical direction to a height of 1000 m, above which the grid spacing remains constant up to 5000 m. The topography of the surface is flat and the urbanized area (the city's model) 10 km in extent is located at the center of the computational domain with an abscissa from 45 to 55 km.

Meteorological initial conditions were determined through specification of the geostrophic wind speeds (3 and 5 m/s) in the west–east direction and the atmospheric thermal stratification characterized by a value of 3.5 K/km for the potential temperature.

On the ground, the mean departure temperature Θ_g from a reference temperature T_0 was given in the form

$$\Theta_g(x, 0, t) = 6 \text{ Sin } (\pi t/43200), \qquad (11a)$$

where t is the current time in seconds. This is the only time-dependent boundary condition of the problem, which simulates a 24-h cycle of heating the Earth's surface by the Sun. The heat island was specified as the temperature contrast with respect to the surface temperature varying according to the same law (11) but with amplitude increased by 4 ^{0}K. At the transverse boundaries, normal derivatives were set equal to zero for all required functions. At the vertical boundary, the required functions satisfied the same boundary condition.

The model's governing equations (1a), (1b), (1c), (2d), (4a), and (5a) written for a two-dimensional case (see Eqs. (14a)– (14e) in the Appendix), along with Eqs. (2e), (4a), and (5a) represented in a two-dimensional form, are solved via the alternating-direction method in combination with the sweep method on a staggered grid. The advective terms of the equations are approximated by the second scheme with upwind differences (Roache, 1976). The distribution of pressure can be calculated simultaneously with the velocity field from the Poisson's diagnostic equation. In this study, where the model is applied to the flow in the ABL with flat topography of the underlying surface, it can be assumed that the hydrostatic approximation is suitable for calculating the distribution of pressure. During computations, the horizontal components of the mean wind are found first through solution of Eqs. (14b) and (14c). The vertical component of the mean wind is calculated via integration of Eq. (14a). Further, the potential temperature, the turbulent kinetic energy, the rate of its dissipation, and the temperature variance are calculated via solution of Eq. (14e) and the three equations written in a two dimensional form for the functions E, ε, and $\langle\theta^2\rangle$. Finally, the pressure is found as a result of integrating the equation for the mean vertical wind velocity (14d) from the lower boundary in the vertical direction. The solution independent of a computational grid is obtained for a 120 × 50 grid. The time step was chosen from the condition that the accuracy remains invariant, and computations were performed with a time step equal to 0.625 s.

4. NUMERICAL STUDY OF URBANIZED SURFACE EFFECT ON THE BOUNDARY LAYER STRUCTURE

In this section, the results of simulation for the simple case described above are compared to the available data of measurements of turbulent momentum and heat fluxes, turbulent kinetic energy, and temperature. Despite a simplified parameterization of the urban surface and a significant scatter of the data, it is possible to reveal some common properties in observations of the urban ABL that must be reproduced by the present model and parameterization. For this purpose, the behavior of the vertical profiles of ABL characteristics at the center of the urbanized area (city) is analyzed below.

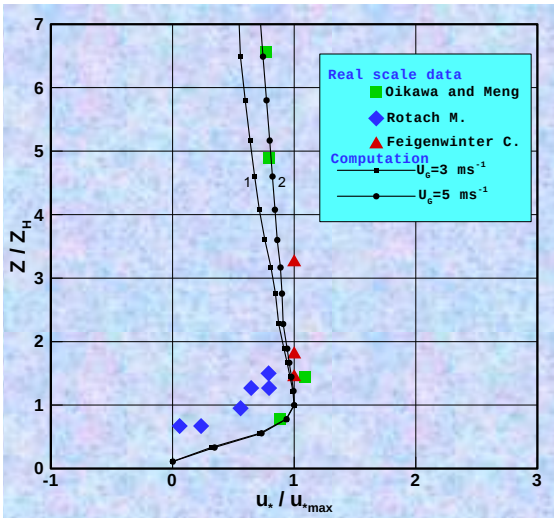

Figure 3. Vertical profiles of the "local" friction velocity u_* (defined as $\left(\langle uw\rangle^2 + \langle vw\rangle^2\right)^{1/4}$) at the center of the urbanized area that are normalized by its maximum value. Different symbols show measurement data: ◆-(Rotach, 1991, 1993, 1995), ■-(Oiakawa and Meng, 1995), and ▲-(Feigenwinter, 1999) Lines *1* and *2* correspond to U_G = 3 m/s and U_G = 5 m/s, respectively. The vertical coordinate Z is normalized by the mean height of buildings in the urbanized area Z_H.

4.1 *Turbulent Momentum*

To verify a numerical model for the urban ABL, the data of measurements and observations available in the literature are employed. The field observations of the structure of turbulence inside and outside the urban canopy layer (Rotach 1991, 1993, 1995) were

carried out in Zurich (Switzerland). The measurements were taken in the central flat area of the city, with a fairly regular arrangement of buildings whose average height is no greater than 20 m.

The values of local friction velocity at different heights are calculated in terms of the Reynolds tangential stresses as

$$u_* = \left(\langle uw \rangle^2 + \langle vw \rangle^2 \right)^{1/4} \qquad (12a)$$

Figure 3 shows the vertical profile of the normalized local friction velocity obtained via the numerical model. In this figure, observational data are depicted as functions of the normalized coordinate Z/Z_H, where Z_H is the average height of a building in the urban canopy layer. All data are normalized by the maximum local friction velocity $u_{*\max}$. These data show a maximum at a height approximately equal to twice the average height of a building and substantially smaller values inside the urban canopy layer. The area below the maximum is usually referred to as the roughness sublayer. Since there is no reliable information about the time of measurements and meteorological conditions for the data obtained by different authors, the calculated values of the friction velocity were averaged over all calculations during their 24-h cycle. As is seen in the figure, the calculated friction velocity increases with height from the underlying surface, reaches a maximum value at the height larger than Z_H, then decreases slightly with increasing height. Such a behavior is consistent with the Monin–Oboukhov similarity theory of the surface layer (the layer of constant flow). The small decrease with increasing height is in good agreement with observational data (Oikawa and Meng, 1995; Feigenwinter, 1999). The extensive data set of measurements in the cities is presented in review of Roth (2000) for the ratio of the local friction velocity u_* to the mean velocity of horizontal wind (six groups of data). The calculated profile of u_*/U (squares in Fig. 4) has a maximum near the top of the building and then decreases with increasing height, reaching a value close to 0.1 at a height of about a fourfold average height of the building. The profiles calculated for two values of the geostrophic wind (3 and 5 m/s) are in good agreement with observational data.

The simulated results presented in these two figures show that the modified model of turbulence for the ABL and a more realistic model of urban roughness (Fig. 2b) are able to reproduce the vertical profiles of both the turbulent momentum flux and the mean velocity of horizontal wind that are consistent with observational data.

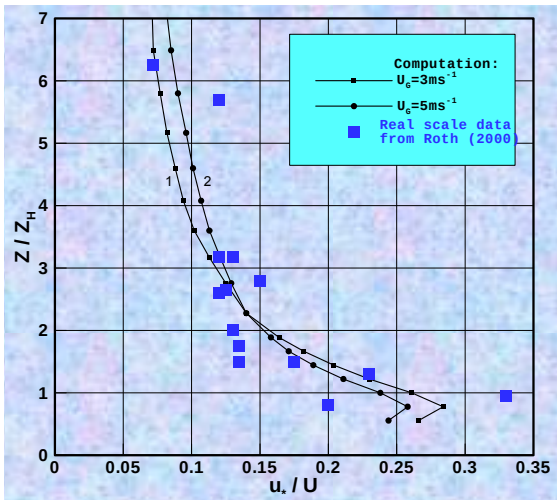

Figure 4. Vertical profiles of the ratio of the local friction velocity u_* to the average horizontal wind velocity at the center of the urbanized area. The symbols correspond to the data of different authors' measurements presented in Fig. 1b of (Roth, 2000). The other notation is the same as in Fig. 3.

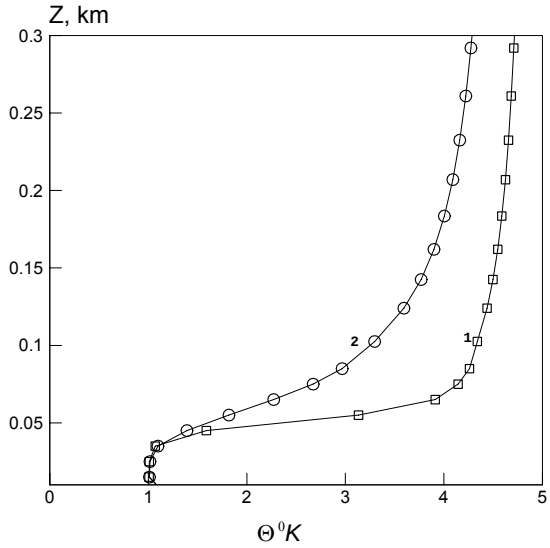

Figure 5. Vertical profile of the deviation of potential temperature for the time 03:00 at the center of an urban heat island (x = 50 km): simulation at the geostrophic wind speed (*1*) U_G = 3 m/s and (*2*) U_G = 5 m/s.

4.2 *Temperature*

The vertical profiles of the deviation of the potential temperature (see the explanation in section 8.1 of the Appendix) in the nighttime ABL (03:00) at the cen-

ter of an urbanized surface are calculated with the modified three-parameter model of turbulence for the ABL and are shown in Fig. 5 for low (3 m/s) and high (5 m/s) geostrophic wind speeds. Comparison with the results of measurements over Sapporo (Japan) exhibits good qualitative agreement with a measured profile of potential temperature (see profile 18U in Fig. 5a of Uno and Wakamatsu (1992) both inside and outside the urban canopy layer. The measurements of series 18U recorded a raised inversion with its base at a height no greater than 60 m. The existence of the elevated nighttime inversion is similar to that over the convective mixed layer; however, the nature of atmospheric stability and turbulence inside the corresponding layers is different (Uno and Wakamatsu, 1992).

4.3. *Turbulent Structure of Urban Atmospheric Boundary Layer*

The structure of turbulence in the boundary layer over an urbanized surface is represented by the profiles of TKE (Fig. 6), standard deviation of the vertical velocity (Fig. 7), and vertical turbulent heat flux (Fig. 8).

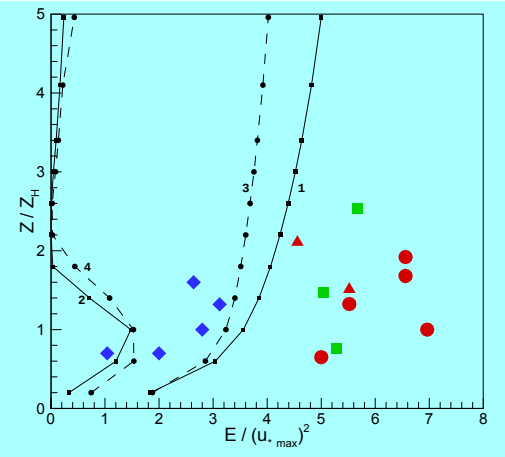

Figure 6. Vertical profiles of the turbulent kinetic energy at the center of the urbanized area that are normalized by the maximum value of the friction velocity squared: simulation at the geostrophic wind speed (solid lines) U_G = 3 m/s and (dashed lines) U_G = 5 m/s; results of simulation for the time (*1*, *3*) 12:00 and (*2*, *4*) 24:00. Different symbols show measurement data: ◆- (Rotach, 1991; 1993; 1995), ■- (Oikawa and Meng, 1995), ▲- (Feigenwinter, 1999), and ●- (Louka et al., 2000).

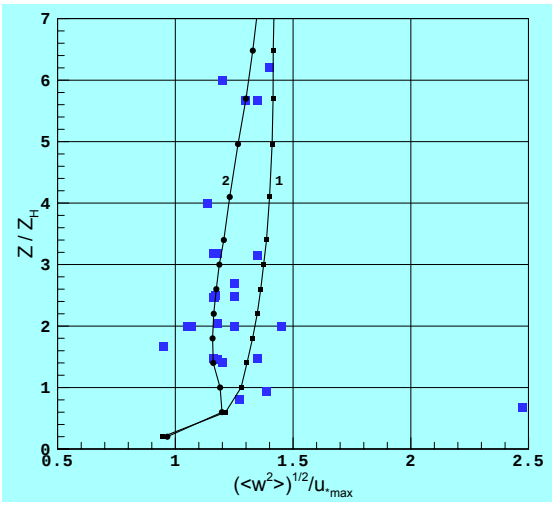

Figure 7. Vertical profile of the standard deviation for the vertical velocity at the center of the urbanized area: simulation at the geostrophic wind speed (*1*) U_G = 3 m/s and (*2*) U_G = 5 m/s. The symbols denote the measurement data (see, Roth, 2000).

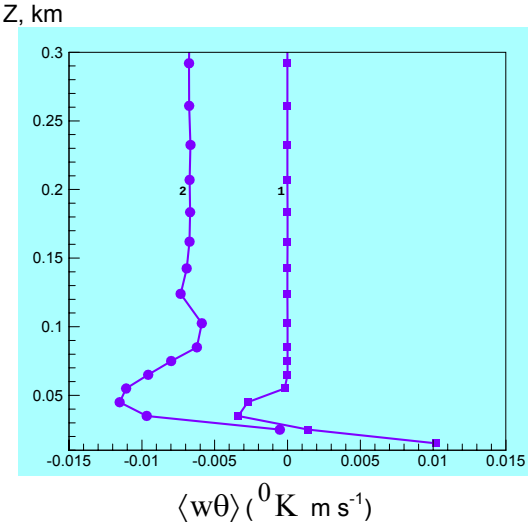

Figure 8. Vertical turbulent heat flux at the center of the urbanized area for the time 03:00: simulation at the geostrophic wind speeds (*1*) U_G = 3 m/s and (*2*) U_G = 5 m/s.

Figure 6 shows the TKE vertical profiles normalized by the maximum friction velocity squared (see the definition in Section 4.1) at the center of an urbanized surface that are simulated for the (instantaneous) moments 12:00 and 24:00. The same figure presents some results of different databases of urban measurements (Rotach, 1991; 1993; 1995; Oikawa and Meng, 1995; Feigenwinter, 1999; Louka et al., 2000). These measurements are carried out for different

morphologies of urban roughness and under different meteorological conditions. The scatter of the measurement data is significant. Some data show a decrease in the TKE in the canopy layer relative to its value above this layer in accordance with a large amount of data of measurements and simulations in the vegetation layer (Raupach et al., 1991). With certain restrictions, these data can be considered similar to those obtained over the canopy layer (buildings) characterized by another effect of mechanical factors on the flow. The numerical results obtained in this study have a correct behavior in the canopy layer and above it. In any case, it is believed that the effect of TKE decreasing in the canopy layer is reproduced by the model. Note that the three-parameter model of thermally stratified turbulence yields satisfactory results when data obtained under controlled conditions of a laboratory experiment are used (Kurbatskii, 2001; Kurbatskii and Kurbatskaya, 2001) and adequately describes the TKE behavior for different states of atmospheric stability. The day-night difference of behaviour of the TKE is difficult to explain because of a wide scatter of the observational data.

The profile of standard deviation of the vertical velocity $\sigma_W / u_{*\max}$ is shown by the solid line in Fig. 7 along with the data of measurements (eight data groups) presented in review of Roth (2000; fig. 2f).These data are depicted by the symbols (blue squares).

From the considerations stated in Section 4.1, Fig. 7 shows the modeling results averaged over all calculations during their 24-h cycle. We note that the calculated profiles are close to the center of the range of data scatter. The normalization is performed with the friction velocity averaged over all values calculated for 24 h (by the same reasoning as in Section 4.1). Thus, it may be inferred that, for this structure characteristic of the turbulence field, this ABL model gives results that are in satisfactory agreement with observational data.

The calculated profiles of vertical heat flux (Fig. 8) are qualitatively consistent with the profiles measured over Sapporo (Uno and Wakamatsu. 1992). Although the measurement data are characterized by a rather wide scatter, a marked minimum near the inversion boundary is present in the data of Uno and Wakamatsu (1992) in Fig. 7 for the chosen time (03:00). The flux gradient changes sign, thus pointing to the heat flux directed downward from the base of the elevated inversion layer.

4.4. *Effect of an Urbanized Surface on Mesoscale Flow*

The results of the previous section relate primarily to the behavior of flow near an urbanized surface and show that the modified three-parameter model is able to reproduce some important characteristics recorded during observations in cities.

This section analyzes the results associated with the effect of urban roughness on the global structure of the ABL to find out to what extent the results obtained with the proposed ABL model are in agreement with observational data and other calculations. Situations with both a weak geostrophic wind, when thermal-stratification effects are of greatest importance and a strong geostrophic wind are discussed.

The numerical results presented in Figs. 3–9 are obtained for two values of the geostrophic wind speed: U_G = 3 m/s and U_G = 5 m/s. On the one hand, such wind-speed values are chosen for a qualitative comparison of the results of this test with the results of the same test of Martilli et al.(2002), where the one-parameter turbulence model is used to calculate all turbulent momentum and heat fluxes with an isotropic effective coefficient of turbulent exchange and with the initiation of an urban heat island via determination of the temperature of the underlying surface from the solution of the equation of heat balance at the surface with consideration for all heat fluxes at the surface, including radiative fluxes.

The results of this test are obtained from a physically more correct calculation of all turbulent fluxes (of momentum and heat) and with the initiation of an urban heat island through specification of the temperature difference between the city and its environs. On the other hand, a small difference between the values of the geostrophic wind speed (3 and 5 m/s) can provide a certain idea of the sensitivity of the improved model for an urban ABL to small variations in the geostrophic wind speed U_G (in particular, for such an integral characteristic as the ABL height above the city).

4.4.1. Daytime ABL. The calculated vertical section of potential temperature at noon (12:00 of a diurnal cycle of modeling the evolution of the urban ABL) in Fig. 9a clearly shows a vertical heated-air column developing over the city and being advected downwind by the synoptic flow: sensible heat fluxes in the city are greater than those in its environs (rural area). This effect, along with the strong turbulence generated by the city's rough structure, increases the height of the boundary layer, as is shown in the figure by the dashed line, from about 800 m in the city's environs to 1.5 km over the city. (The ABL height is defined (Martilli et al., 2002) by the height of the layer of the model's computational grid at which the TKE is smaller than or equal to 0.01 $m^2 s^{-2}$.) Such an increased boundary layer over the city as compared to that in the environs was observed, for example, by Spanton et al. (1988). The horizontal wind field in Fig. 9b shows low wind speeds near the surface of the city.

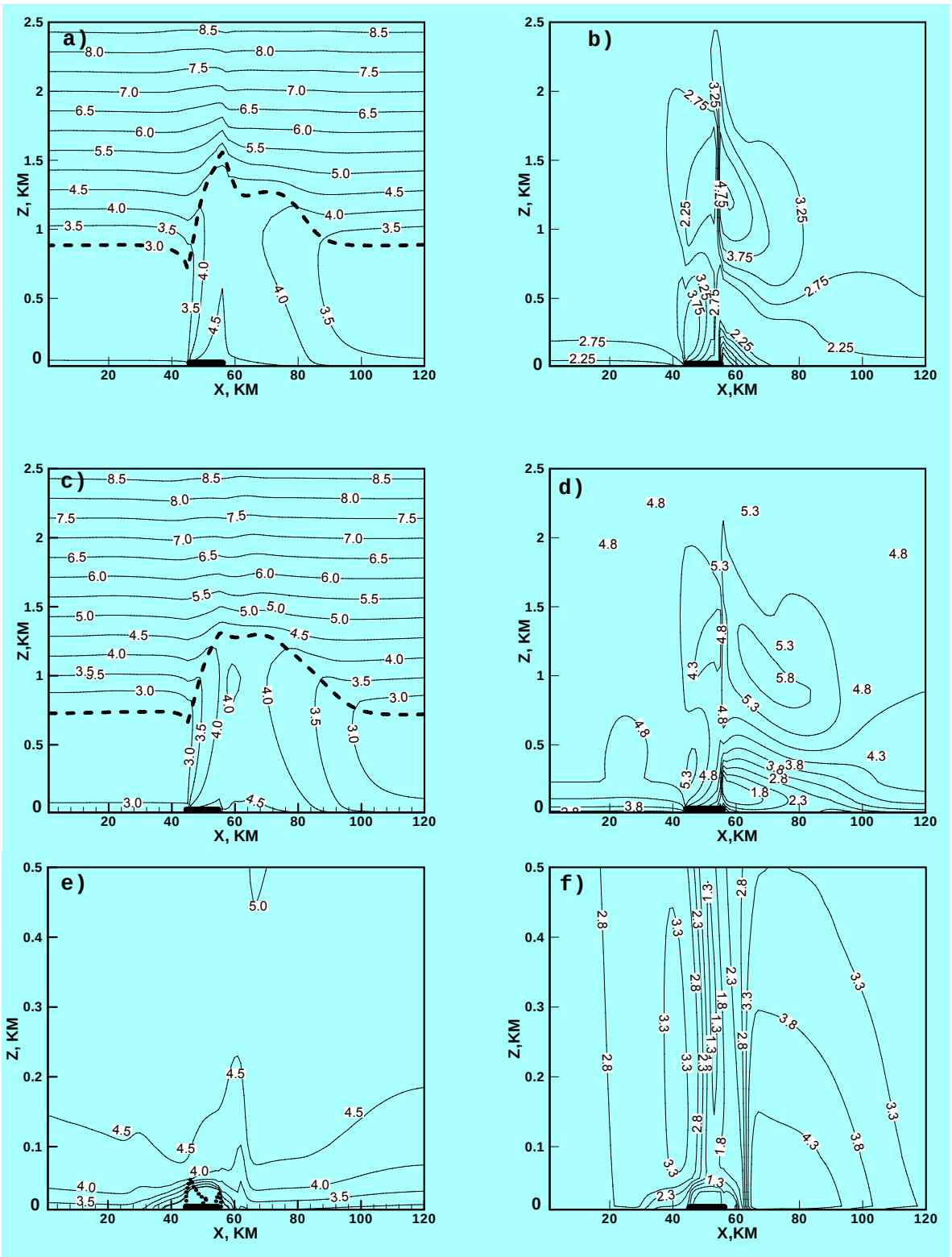

Figure 9. Calculated (a, c, e) vertical sections of the deviation of potential temperature (K) and (b, d, f) horizontal wind speed (m/s) for the time (a, b, c, d) 12:00 and (e, f) 24:00 at the geostrophic wind speed (a, b, e, f) 3 and (c, d) 5 m/s. On the sections of potential temperature, the dashed line shows the ABL height, which is determined as the level at which the TKE is smaller than 0.01 m^2/s^2. The segment of the heavy line with the abscissa from 45 to 55 km marks the location of the urbanized area (city).

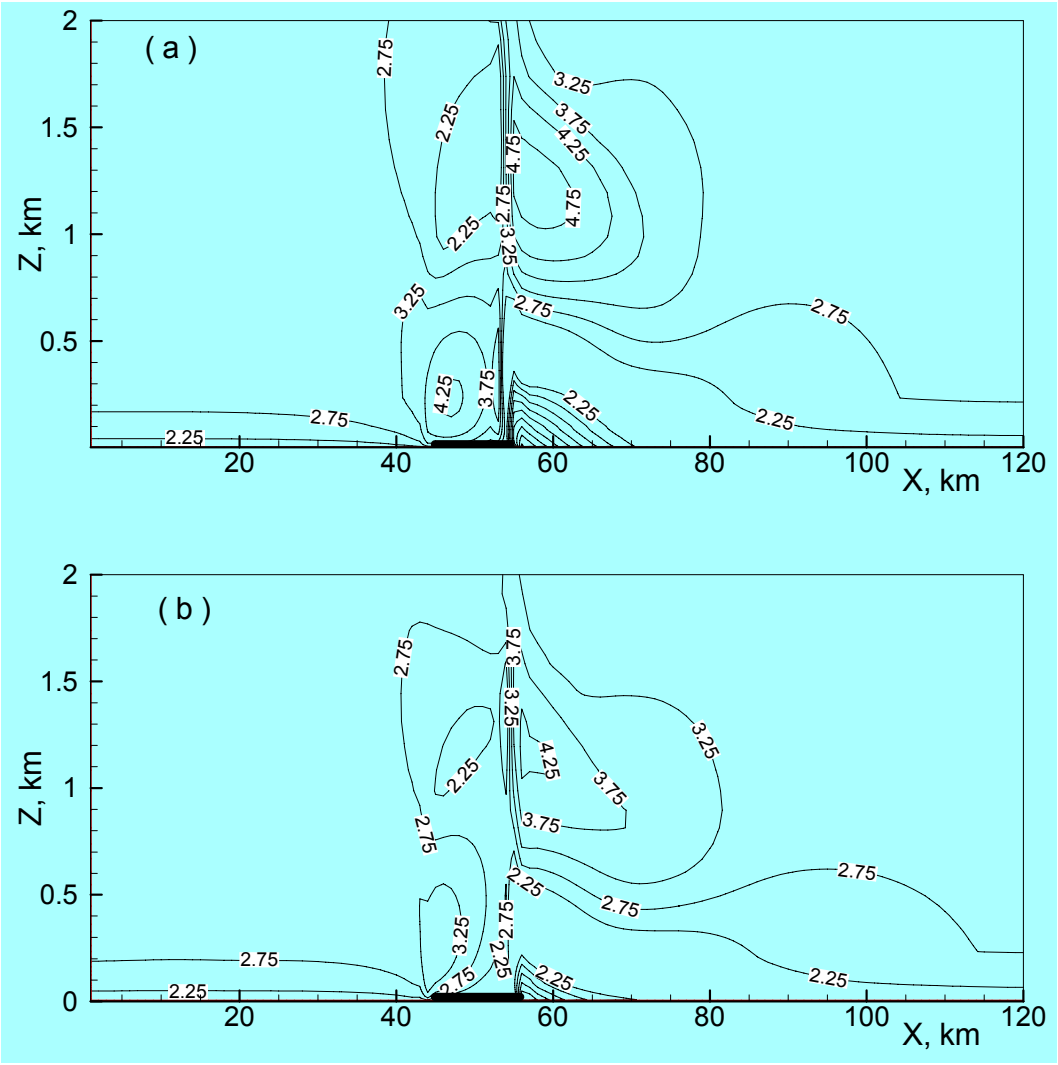

Figure 10. Calculated vertical sections of horizontal wind speed (m/s) for the time 12:00: (a) - simulation with the classical MOST approach and (b) - simulation with the parameterization of urban roughness. The thick line on the abscissa between 45 km and 55 km indicates the location of the urbanized area (city).

It possible to make some quantitative estimation of the wind speed changes above city influenced by the mechanical (urban roughness) and thermal (the urban heat island effect) inhomogeneity of the urbanized area. Fig. 10(a) shows results of the simulation with only the classical MOST approach. The simulation with the parameterization of the urban roughness in Fig. 10(b) is represented. It follows from these figures that the urban roughness reduces the wind speed above the city by about 24 percent, as compared with the classical MOST approach. Thus, the increase in wind speed above the city most is likely connected with the urban heat island effect. A similar modification of the wind speed above the city was probably simulated (for example, Martilli et al., 2002).

The influence of this effect on the structure of the ABL with usual roughness (Fig. 2a) and with a heat island during the implementation of the same simple two-dimensional test is shown by Kurbatskii (2005). Other things being equal, the height of the boundary layer turns out to be greater in the presence of longitudinal turbulent diffusion of heat than in its absence. Indeed, the calculated results shown in Fig.11 allow estimating the effect of the longitudinal turbulent heat diffusion on the boundary layer characteristics. It is seen from Fig.11 that the height of the boundary layer above city (marked by the dashed line) in the presence of diffusion is higher than in its absence. The longitudinal diffusion transports the heat into the column of the heated air above the city (heat spot), which increases the TKE generation due to the fluctuating buoyancy force and favors the increase of the PBL height.

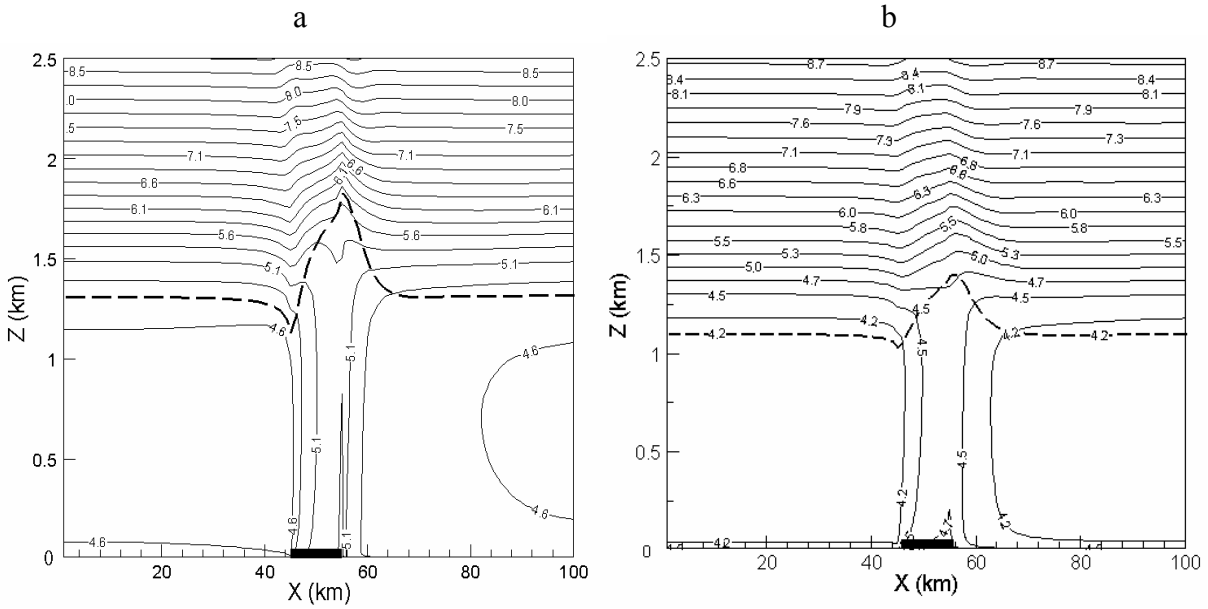

Figure 11. Vertical sections of the deviations of the potential temperature, calculated taking into account (*a*) and neglecting (*b*) the longitudinal turbulent heat diffusion at 12:00 a.m. (U_G=5 m/s).

Figures 12*a* and 12*b* depict the vertical sections of the deviations of the potential temperature (*a*) and the mean wind field (*b*) calculated with the mesoscale model, described in this paper, for 12:00 a.m. in the diurnal cycle of modeling. Figures 3*c* and *d* show the same sections over the modeled heat island obtained in [5] with a single-parameter model of turbulence (all turbulent momentum and heat fluxes are determined by the gradient Boussinesq model with the turbulent viscosity coefficient) and parameterization of the main factors of the heterogeneous urban surface (head resistance of buildings, radiative processes in city canyons). In both of the cases, the same test for the 2D area (see Subsection 3.1 above) and the same initial distribution of the potential temperature and the geostrophic wind were used.

The results of both tests cannot be compared quantitatively because of different parameterization of the effect of the urban heat island and the effects of the urban roughness, which significantly change the structure of the flow directly in the layer of obstacles, a part of the urban atmospheric boundary layer adjacent to the surface. However, the large-scale air circulation within the domain of integration in both of the numerical tests can be compared qualitatively. It should be noted, in addition, that the verification of one or another parameterization of the turbulent exchange processes within urban surfaces always present severe difficulties either due to the absence of field measurements or due to the heterogeneity of urban surfaces, which is always very high. The vertical sections of the field of the potential temperature are similar.

The wind velocity (Figs. 12*b* and *d*) increases over the city, because the vertical temperature gradient between the air above the city and the air above the city surroundings generates the thermal circulation, which can be seen from the isotachs of the vertical velocity in Fig.14. In addition, the pressure gradient, caused by higher temperatures over the city, has here the same sign as the advection. Along with the effects of friction near the surface, this leads to the lower wind values near the urban surface and higher values above it. The minimum in the wind velocity downstream out of the city arises because the pressure gradient and the advection of the synoptic wind have the opposite signs in this area. The presence of such a "cap" of the warm air above the urban heat island was observed, in particular, in laboratory measurements (Lu et al., 1997) and in numerical investigations (Kurbatskii, 2001).

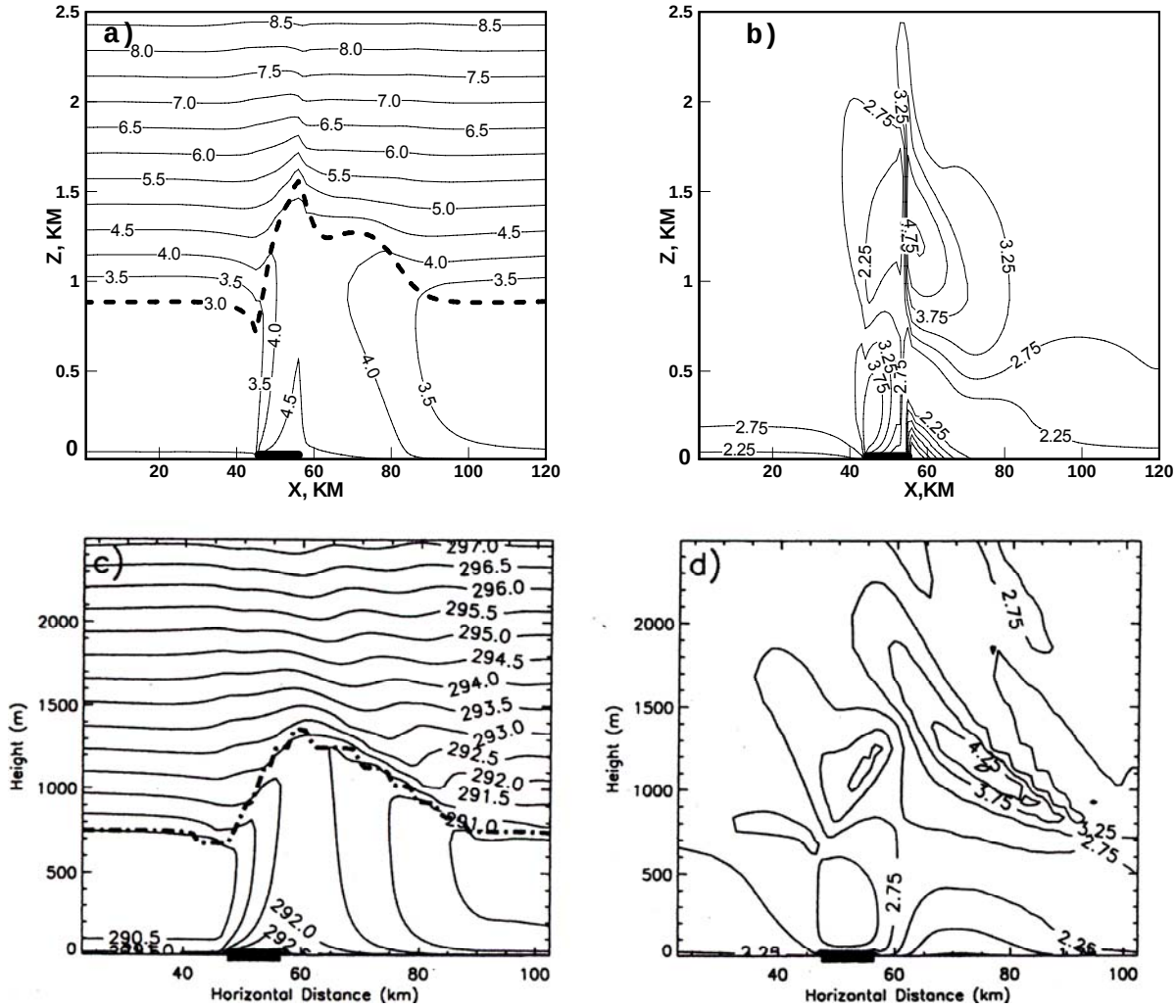

Figure 12. Vertical sections of the potential temperature (a, c) and the mean horizontal wind (b, d) at 12:00 a.m. as calculated in this study (a, b) and in [5] (c, d) ($U_G = 3$ m/s).

5. COMPARISON BETWEEN $E-\varepsilon-\langle\theta^2\rangle$ and $k-\varepsilon$ TURBULENCE MODELS

As noted in the introduction, two turbulence models commonly used for simulating the urban boundary layer include standard $k-\varepsilon$ model modified for effects of buoyancy on vertical turbulent transport (see, for example, Vu et al., 2002), and a traditional approach (see, for example, Martilli et al., 2002) based on the one-parameter turbulence model. In this model, the turbulence length scale is found as a function of the vertical coordinate based on some assumptions. Such an approach does not take into account either anisotropic transport in vertical and horizontal directions, or effects of buoyancy on vertical turbulent transport.

Computations of wind field, temperature and turbulent quantities inside the urban boundary layer allow detecting differences in the turbulent transport modeled with the three-parameter $E-\varepsilon-\langle\theta^2\rangle$ model and standard K-theory]. For this purpose, values of "turbulent exchange coefficients" $K_M = -\langle uw\rangle/(\partial U/\partial z)$ and $K_H = -\langle\theta w\rangle/(\partial\Theta/\partial z)$ are computed diagnostically in the same way as for the horizontal homogeneous atmospheric boundary layer (Mellor and Yamada, 1974), and the results are shown in Fig. 13a,b. As can be clearly seen in Fig. 13a, b, negative values of K_M and K_H are predicted in the region of turbulent thermal circulation on the leeward side of the urbanized area (Fig. 14). However, their negative values are also predicted in the

lower urban boundary layer part for K_M and upper urban boundary layer part for K_H .

Regions of negative values of K_M and K_H explicitly indicate non-local character of the turbulent transport which can not be described using simple one- or two-parameter turbulence models. In these two models, it is difficult to correctly account for effects of buoyancy on the turbulent transport of momentum, mass and heat. For example, figure 15 shows that the 'standard' $k-\varepsilon$ model underpredicts values of the vertical turbulent heat flux when compared with the $E-\varepsilon-\langle\theta^2\rangle$ model and fully explicit anisotropic model for turbulent fluxes of momentum, mass and heat.

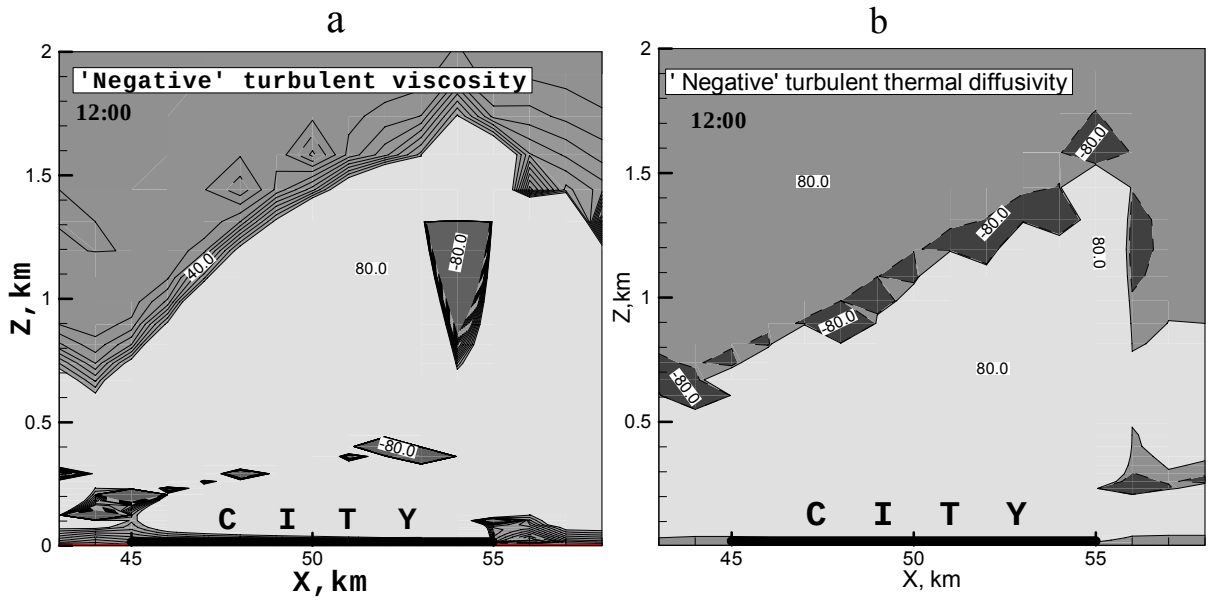

Figure 13. Momentum (a) and heat (b) turbulent exchange coefficients for *Urban* simulation at noon. Results are for the case with $3\,\mathrm{m\,s^{-1}}$ geostrophic wind.

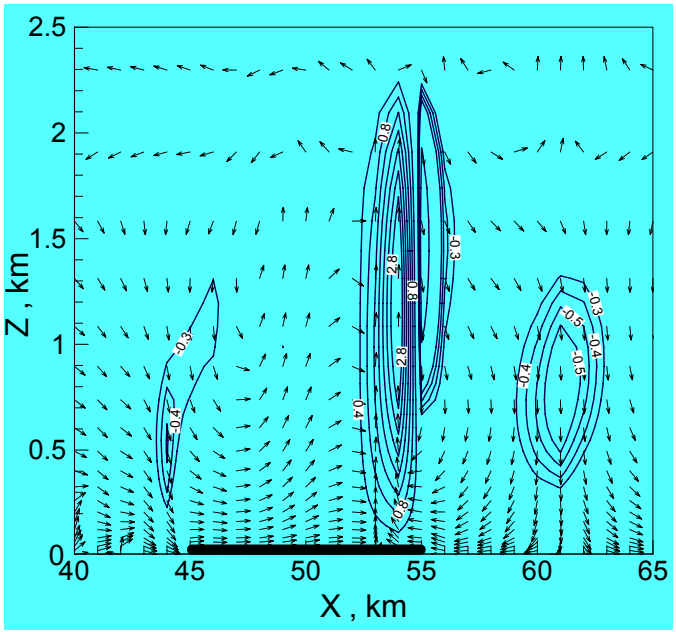

Figure 14. Velocity vectors and isotachs ($\mathrm{ms^{-1}}$) for vertical velocity at 12:00 (*noon*) in the diurnal cycle of simulation for the geostrophic wind speed $\mathrm{U_G} = 3\,\mathrm{m\,s^{-1}}$.

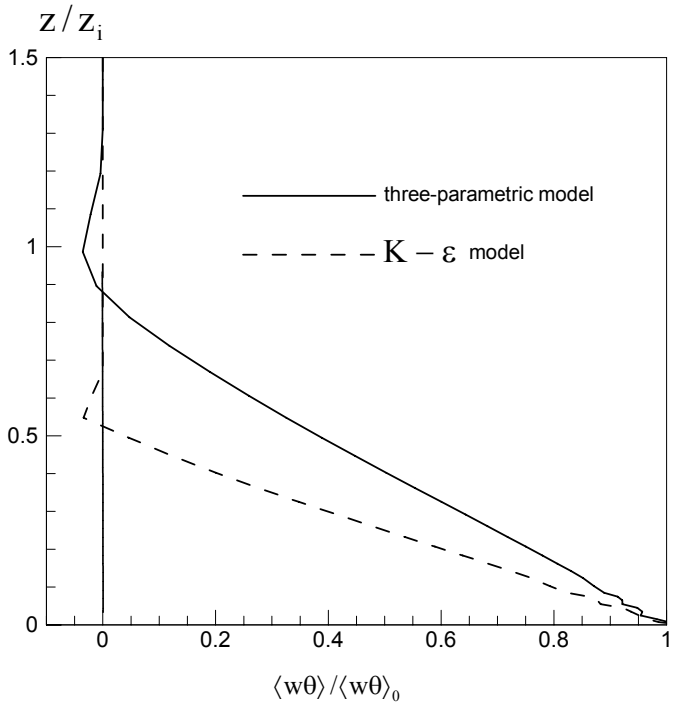

Figure 15. Vertical turbulent heat flux in a point in the center of the city at 12:00 (*noon*) in the diurnal cycle of simulation for the geostrophic wind speed $U_G = 3\,m\,s^{-1}$ computed by means of 'standard' $k-\varepsilon$ model and the three-parametric $E-\varepsilon-\langle\theta^2\rangle$ turbulence model with the fully explicit anisotropic model for turbulent fluxes. The fluxes normalized on the maximum value of $\langle w\theta\rangle_0$.

6. DISPERSION OF PASSIVE TRACER ABOVE CITY: NUMERICAL TEST

6.1. *Introduction*

For a typical urbanized surface (city), a significant contribution to the total emission of pollutants is made by a large number of relatively weak sources located mainly near the surface. As a result, effects of turbulence in the urban canopy layer become important for modeling of pollution dispersion in a city environment, and they should be included in urban dispersive models for improving the quality of forecasting (Rotach, 1999). In mesoscale modeling of a structure of wind and temperatures fields, the city can be represented by a heated "spot" surrounded by its neighborhoods (Fernando et al., 2001), and effects of urban roughness on turbulent transport of momentum, heat and mass can be parameterized (Vu et al., 2002; Martilli et al., 2002). Developing internal boundary layer at the "city-rural area" interface has a mechanical as well as a thermal origin. Because of this, it is desirable to preserve anisotropy of turbulent transfer in vertical and horizontal directions which cannot be adequately reproduced by traditionally used one-and two-parametric models of a turbulent atmospheric boundary layer (see, for example, [3, 5]). The improved mesoscale model of a turbulent atmospheric boundary layer with anisotropic expressions for turbulent fluxes of momentum and heat, and parameterization of urban roughness effects on turbulent transport allows to obtain wind and temperature fields above the urbanized surface predicting increase in wind speed above the city, which qualitatively agrees with observation data (Bornstein and Johnston, 1977). The model also takes into account the impact of the longitudinal turbulent diffusion of a scalar (heat and concentration) resulting from the horizontal thermal inhomogeneity created by city and its neighborhoods on integral characteristics of an urban boundary layer. The present section formulates the turbulent diffusion mesoscale model where turbulent fluxes of concentration are defined by completely anisotropic algebraic expressions. This model is used for computing of passive tracer dispersion above the city in a simple two-dimensional (2D) case simulating 24-hour evolution of the atmospheric boundary layer above the city.

6.2. *Turbulent Diffusion Model for Pollution Dispersion*

The baseline mesoscale model of turbulent atmospheric boundary layer is expanded to include atmos-

pheric dispersion of a passive contaminant by adding equations for mean concentration $C(x_i,t)$, turbulent contaminant flux $f_j \equiv < u_i c >$ and correlation $< c\theta >$.

Numerical results from validations of differential and algebraic models for turbulent concentration fluxes used in modeling of passive tracer dispersion above an urban heat island under conditions of night-time atmospheric boundary layer (weak wind, stable stratified atmosphere) have shown (Raupach et al., 1991) that the algebraic model for turbulent concentration fluxes provides acceptable in accuracy results. Such a model is formulated by simplifying closed differential transport equation for the turbulent scalar flux $\langle u_i c\rangle$ under the same local-equilibrium turbulence assumption applied in section 2. 3 for simplification of equations for turbulent momentum (Reynolds stresses) and heat flux.

$$\frac{D < u_i c >}{Dt} - \frac{\partial}{\partial x_k}\left\{\alpha_{1s}\frac{E}{\varepsilon} < u_k u_l > \frac{\partial < u_i c >}{\partial x_l}\right\} =$$
$$- < u_i u_j > \frac{\partial C}{\partial x_j} - < u_j c > \frac{\partial U_i}{\partial x_j} -$$
$$+\alpha_{3c} g_i \beta < c\theta > - g_i \beta < c\theta > -$$
$$-\alpha_{1c}\frac{\varepsilon}{E} < u_i c > + \alpha_{2c} < u_j c > \frac{\partial U_i}{\partial x_j}. \qquad (13a)$$

This approach assumes that the left hand side of (13a) can be neglected and the following algebraic equation for $f_j \equiv \langle u_i c\rangle$ is obtained,

$$A_{ij}\cdot f_j = -\frac{E}{\varepsilon}(b_{ij} + \frac{2}{3}E\delta_{ij})\frac{\partial C}{\partial x_j} +$$
$$+(1-\alpha_{2C})\beta g \delta_{i3}\frac{E}{\varepsilon}\langle c\theta\rangle \qquad (13b)$$

where $b_{ij} = \langle u_i u_j\rangle - (2/3)E\delta_{ij}$ is the traceless Reynolds stress tensor.

The closed prognostic equation of (13c) for correlation $\langle c\theta\rangle$ (Enger, 1986) is,

$$\frac{D\langle c\theta\rangle}{Dt} - Diff_{\langle c\theta\rangle} = -\langle u_j\theta\rangle\frac{\partial C}{\partial x_j} - \langle u_j c\rangle\frac{\partial \Theta}{\partial x_j} -$$
$$-\alpha_{3C}\frac{\varepsilon}{E}\langle c\theta\rangle, \qquad (13c)$$

where $\mathrm{Diff}_{\langle c\theta\rangle}$ is the turbulent transfer term, also reduced under the weak-equilibrium turbulence approach to the algebraic equation,

$$\langle c\theta\rangle = -\frac{1}{\alpha_{3C}}\frac{E}{\varepsilon}\left(\langle u_j c\rangle\frac{\partial\Theta}{\partial x_j} + \langle u_j\theta\rangle\frac{\partial C}{\partial x_j}\right) \qquad (13d)$$

Substituting (13d) into (13b) yields the algebraic equation for flux concentration f_j

$$A_{ij}\cdot f_j = -\frac{E}{\varepsilon}\{(b_{ij} + \frac{2}{3}E\delta_{ij}) +$$
$$+\frac{(1-\alpha_{2C})}{\alpha_{3C}}\beta g\delta_{i3}\frac{E}{\varepsilon}h_j\}\frac{\partial C}{\partial x_j} \qquad (13e)$$

where

$$A_{ij} = \alpha_{1C}\delta_{ij} + \frac{E}{\varepsilon}\frac{\partial U_i}{\partial x_j} +$$
$$+\left(\frac{E}{\varepsilon}\right)^2\frac{(1-\alpha_{2C})}{\alpha_{3C}}\beta g\delta_{i3}\frac{\partial\Theta}{\partial x_j}. \qquad (13f)$$

Anisotropic expressions for vertical $\langle wc\rangle$ and horizontal $\langle uc\rangle$ turbulent fluxes of concentration are derived by means of symbolical algebra from (13e) in following form,

$$-\langle wc\rangle = \frac{1}{D}\left(\alpha_{1C}\frac{E}{\varepsilon}\left[\langle w^2\rangle + \alpha^*\lambda_1\langle w\theta\rangle\right]\right)\frac{\partial C}{\partial z} +$$
$$+\frac{1}{D}\left(\alpha_{1C}\frac{E}{\varepsilon}\left[\langle uw\rangle + \alpha^*\lambda_1\langle u\theta\rangle\right]\right)\frac{\partial C}{\partial x}, \qquad (13g)$$
$$-\langle uc\rangle = \frac{1}{D}(\frac{E}{\varepsilon}[\langle u^2\rangle\lambda_2 + \frac{E}{\varepsilon}\frac{\partial U}{\partial z}(\langle uw\rangle +$$
$$+\alpha^*\lambda_1\langle u\theta\rangle)])\frac{\partial C}{\partial x} + \frac{1}{D}(\frac{E}{\varepsilon}[\langle uw\rangle\lambda_2 +$$
$$+\frac{E}{\varepsilon}\frac{\partial U}{\partial z}\left(\langle w^2\rangle + \alpha^*\lambda_1\langle w\theta\rangle\right)])\frac{\partial C}{\partial z}. \qquad (13h)$$

In these expressions, $\alpha^* = (1-\alpha_{2C})/\alpha_{3C}$,
$\lambda_1 = \beta g(E/\varepsilon)$,
$\lambda_2 = \alpha_{1C} + \frac{E}{\varepsilon}\frac{\partial W}{\partial z} + \alpha^*\lambda_3\frac{\partial\Theta}{\partial z}$,
$\lambda_3 = \beta g(E/\varepsilon)^2$.

In From (13g) and (13h) the equation for mean concentration

$$\frac{\partial C}{\partial t} + \frac{\partial}{\partial x}C\cdot U + \frac{\partial}{\partial z}C\cdot W =$$
$$-\frac{\partial}{\partial z}\langle wc\rangle - \frac{\partial}{\partial x}\langle uc\rangle \qquad (13i)$$

is reduced to the closed form after neglecting molecular diffusion at higher Reynolds numbers. The numerical constants of diffusion models (13g) – (13i) are: $\alpha_{1C} = \alpha_{3C} = 3,28$, $\alpha_{2C} = 0,4$.

6.3. *Results of Numerical Modeling of Passive Tracer Dispersion above City*

The computed tracer concentration in the city centre at the lowest modeled level during 48-hour cycle of simulating the urban boundary layer evolution is presented on fig. 16. As expected, the concentrations are higher during the night than during the day, because the nocturnal boundary layer is much thinner than the diurnal one. It should be noted here that the overprediction of primary pollutants during the night in urban areas, as compared to the measurements, is fairly common for Eulerian photochemical models, especially under low wind conditions (Moussiopoulos et al., 1997). This problem can be linked to an inappropriate reproduction of the nocturnal urban heat island.

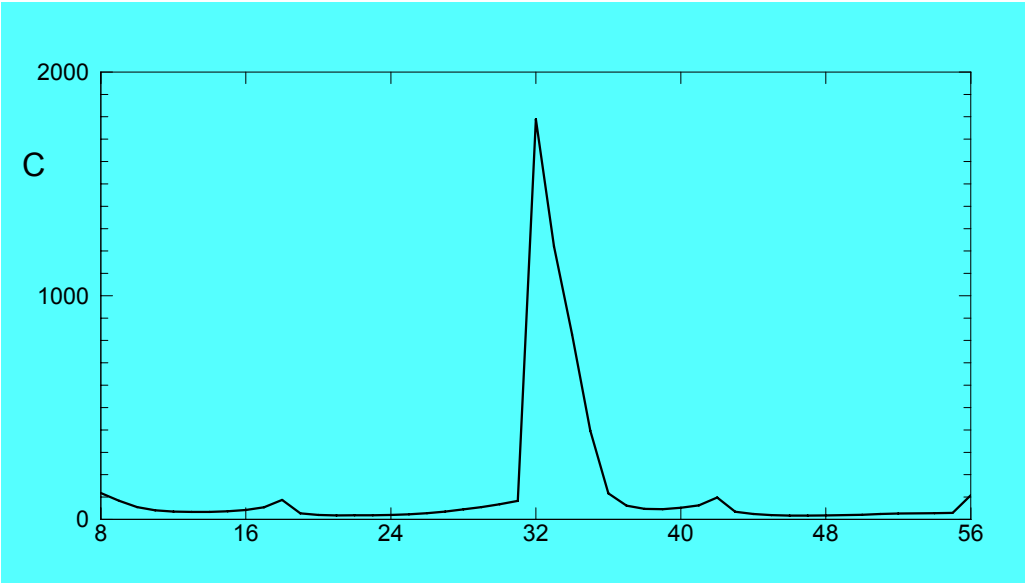

Figure 16. Time evolution of passive tracer surface concentration in the centre of the urban area as computed by the three-parameter turbulence model. Results are for the case with the geostrophic wind $U_G = 3$ m/s.

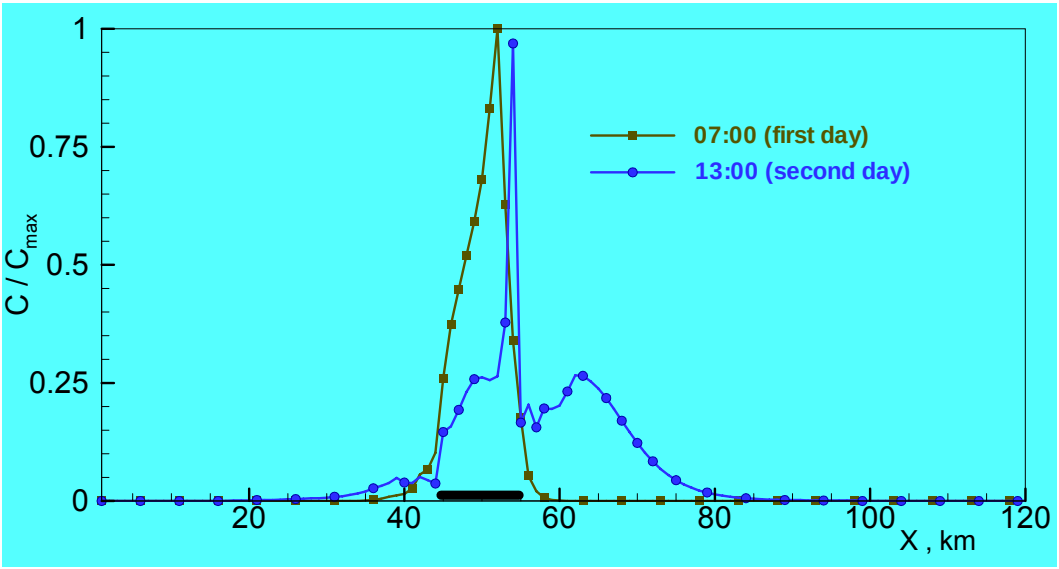

Figure 17. Passive tracer concentration. At the lowest level at 13:00 a.m. of the second day. The city is located between 45 km and 55 km. Results are for the case with the geostrophic wind $U_G = 3$ m/s.

Thus, influence of the urban surface on the day time pollutant concentration away from the city is clearly shown. This result is in qualitative agreement with calculations (Martilli et al., 2002)]. The above-noted behavior of concentration in a vicinity of city's leeward side is caused by the nature of the thermal circulation moved by advection downwind to the leeward side (see also a Figure 14 showing the isotachs of vertical wind speed (arrows show the average wind vector field).

A method of simulating pollutant dispersion in mesoscale atmospheric models is presented in this section. Influence of the urban roughness (buildings) is not explicitly resolved, but their effects on the grid-averaged variables are parameterized. In Eulerian diffusion models, turbulent fluxes of concentration are computed from completely explicit algebraic expressions taking into account the anisotropy of transfer in vertical and horizontal directions. Numerical results of passive tracer dispersion emitted at ground level in the centre of the urban area correctly reflect behavior of concentration near the surface during the 24-hour evolution of the urban boundary layer. Impact of the city on day time concentration of pollution away from it during the second day is correctly predicted by the numerical model.

7. CONCLUSIONS

A three-parameter mesoscale model of explicit anisotropic turbulent fluxes of momentum and heat has been developed in this paper for modeling atmospheric flows over an inhomogeneous underlying surface. An important property of the model lies in the improvement of estimating the processes of transfer in the vertical and horizontal directions under different stratification conditions, which are usually observed in an urban boundary layer. A simple two-dimensional numerical test on the influence of mechanical factors (urban roughness) and thermal factors (effect of an urban heat island) on a global structure of the atmospheric boundary layer has been implemented. This test has shown that the results of numerical simulation are in good qualitative and quantitative agreement with the data of field measurements. The model is able to reproduce turbulent processes within the urban canopy layer and above it with satisfactory accuracy. The formulated model of turbulent fluxes with closure level 3.0 can be potentially used to model the atmospheric boundary layer within the "urban" scale and "mesoscale." The improvement of the model requires a more accurate calculation of heating processes in the urban canopy layer, and this modification of the model is regarded as the aim of our further study. Note that the description of a detailed pattern of urban climate requires measurement data on turbulent quantities within the urban canopy layer. Such data allow a more accurate specification of the desired functions of the three-parameter model at the lower boundary near the surface (at the first computation level), because the use of the approximations of constant fluxes in the surface layer that are based on the Monin–Oboukhov theory does not allow an adequate (to the data of field measurements; see, for example, Rotach, 1993) reproduction of the vertical structure of turbulent fields in the urban canopy layer (from the level of the urban street canyon to heights of 50–100 m). It is clear that a realistic modeling of the dispersion of urban pollutants requires an accurate knowledge of meteorological parameters for this region of the urban ABL, where the pollutants are emitted and where people live. An efficient use of this model for the turbulent ABL requires the specification (from measurement data) of "input" parameters such as the vertical distributions of the three base functions of the model, E, ε, and $\langle\theta^2\rangle$ (for example, in the morning hours for a stably stratified ABL). Testing the potentials of the RANS turbulence model for an urban ABL requires the measurement data on the distributions of a number of quantities, such as the variance of the vertical component of turbulent velocity and the boundaries of surface and raised inversions (including those under the conditions of weakened ABL turbulence in the night and early-morning hours, measurement data on vertical distributions of temperature, turbulent heat flux, TKE, and other parameters).

8. APPENDIX

The Appendix presents the governing system of equations of a turbulent horizontally inhomogeneous thermally stratified ABL for the two-dimensional test under study. Explicit analytic expressions are given for the turbulent momentum and heat fluxes, and numerical values are presented for the constants of the modified three-parameter model of turbulence. Detailed expressions are presented for the parameterization of the effects of urbanized-surface roughness.

8.1. *Governing System of Equations for the Turbulent ABL*

For flows in a planetary boundary layer, some approximations can be used in the governing equations. In (1a), the rotation term can be approximated with the expression

$$-2\varepsilon_{ijk}\Omega_j U_k = f_c \varepsilon_{ij3} U_j$$

where the axes x, y, and z are directed eastward, north-ward, and upward, respectively, and $f_c = 2\Omega\sin\varphi$ is the Coriolis parameter with the angular velocity of the Earth's rotation Ω and latitude φ. The buoyancy effects are taken into account in the Boussinesq approximation, and, for a two-dimensional flow, the system of equations (1a) and (1b) is written as

$$U_x + W_z = 0, \tag{14a}$$

$$U_t + UU_x + WU_z = -\frac{1}{\rho}P_x - \langle wu \rangle_z + fV + \hat{D}_u, \tag{14b}$$

$$V_t + UV_x + WV_z = -\langle wv \rangle_z - fU + \hat{D}_v, \tag{14c}$$

$$W_t + UW_x + WW_z = -\frac{1}{\rho_0}P_z - \langle ww \rangle_z + \beta\hat{\Theta}g, \tag{14d}$$

$$\hat{\Theta}_t + U\hat{\Theta}_x + W\hat{\Theta}_z = -\langle u\theta \rangle_x - \langle w\theta \rangle_z + \hat{D}_\theta. \tag{14e}$$

The dependent variables in (14a)–(14e) are the mean (time averaged) flow velocities U, V and W in the directions of the x, y and z axes, respectively, the mean pressure P, and the mean departure of potential temperature $\hat{\Theta}$ from a reference temperature T_0. The parametric quantities in (14a)–(14e) include the volumetric expansion rate of air β (3.53 ×10^{-3} K^{-1}), the mean air density ρ_0. The lower case letters denote turbulent fluctuations of the corresponding quantities. The Reynolds turbulent stresses τ_{ij} and the turbulent heat flux vector h_j in equations (14a)–(14e) requires modeling. Explicit algebraic models for the Reynolds stresses and the turbulent heat flux are formulated in the next section.

8.2. *Algebraic Expressions for Turbulent Momentum and Heat Fluxes*

From Eq. (9a) with consideration for $b_{ij} = \langle u_i u_j \rangle - \frac{2}{3}E\delta_{ij}$ and from Eq. (10a) for the vector of turbulent heat flux $h_i = \langle u_i \theta \rangle$ the following implicit system of equations for the turbulent momentum and heat fluxes is written in the boundary-layer approximation:

$$\langle u^2 \rangle = \frac{2}{3}E - \frac{\tau}{3}(4\alpha_2 \frac{\partial U}{\partial z}\langle uw \rangle - 2\alpha_2 \frac{\partial V}{\partial z}\langle vw \rangle +$$

$$+2\alpha_3\beta g \langle w\theta \rangle), \tag{15a}$$

$$\langle v^2 \rangle = \frac{2}{3}E - \frac{\tau}{3}(4\alpha_2 \frac{\partial V}{\partial z}\langle vw \rangle - 2\alpha_2 \frac{\partial U}{\partial z}\langle uw \rangle +$$

$$+2\alpha_3\beta g \langle w\theta \rangle), \tag{15b}$$

$$\langle w^2 \rangle = \frac{2}{3}E + \frac{\tau}{3}(2\alpha_2 \frac{\partial U}{\partial z}\langle uw \rangle + 2\alpha_2 \frac{\partial V}{\partial z}\langle vw \rangle +$$

$$+4\alpha_3\beta g \langle w\theta \rangle), \tag{15c}$$

$$\langle uw \rangle = -\frac{\tau}{2}\frac{\partial U}{\partial z}2\alpha_2 \langle w^2 \rangle + \alpha_3\tau\beta g \langle u\theta \rangle, \tag{15d}$$

$$\langle vw \rangle = -\frac{\tau}{2}\frac{\partial V}{\partial z}2\alpha_2 \langle w^2 \rangle + \alpha_3\tau\beta g \langle v\theta \rangle, \tag{15e}$$

$$\langle uv \rangle = -\tau\alpha_2\left(\frac{\partial V}{\partial z}\langle uw \rangle + \frac{\partial U}{\partial z}\langle vw \rangle\right), \tag{15f}$$

$$\langle u\theta \rangle = -\frac{\tau}{\alpha_5}\left(\frac{\partial \Theta}{\partial z}\langle uw \rangle + \alpha_4 \frac{\partial U}{\partial z}\langle w\theta \rangle\right), \tag{15g}$$

$$\langle v\theta \rangle = -\frac{\tau}{\alpha_5}\left(\frac{\partial \Theta}{\partial z}\langle vw \rangle + \alpha_4 \frac{\partial V}{\partial z}\langle w\theta \rangle\right), \tag{15h}$$

$$\langle w\theta \rangle = -\frac{\tau}{\alpha_5}\left(\frac{\partial \Theta}{\partial z}\langle w^2 \rangle - \alpha_4\beta g \langle \theta^2 \rangle\right). \tag{15i}$$

Equations (15a)–(15i) were solved via symbol algebra. Below, we present expressions for those turbulent momentum and heat fluxes that were used in a numerical test to solve system of equations (14a) – (14e):

$$(\langle uw \rangle, \langle vw \rangle) = -K_M\left(\frac{\partial U}{\partial z}, \frac{\partial V}{\partial z}\right), \tag{16a}$$

$$\langle w\theta \rangle = -K_H \frac{\partial \Theta}{\partial z} + \gamma_c, \tag{16b}$$

$$K_M = E\tau S_M, \quad K_H = E\tau S_H, \tag{16c}$$

$$S_M = \frac{1}{D}\{s_0\left[1 + s_1 G_H\left(s_2 - s_3 G_H\right)\right] +$$

$$+s_4 s_5\left(1 + s_6 G_H\right)(\tau\beta g)^2 \frac{\langle \theta^2 \rangle}{E}\}, \tag{16d}$$

$$S_H = \frac{1}{D}\left\{\frac{2}{3}\frac{1}{c_{1\theta}}\left(1 + s_6 G_H\right)\right\}, \tag{16e}$$

where

$$\gamma_c = \frac{1}{D}\left\{1+\frac{2}{3}\alpha_2^2 G_M + s_6 G_H\right\}\alpha_5(\tau\beta g)\left\langle\theta^2\right\rangle. \qquad (16f)$$

is the countergradient term, which is absent in models with closure levels 2.0 and 2.5 (Cheng et al., 2002).

The quantities G_H and G_M are defined as

$$G_H \equiv (\tau N)^2, \quad G_M \equiv (\tau S)^2, \qquad (16g)$$

$$N^2 = \beta g\frac{\partial\Theta}{\partial z}, \quad S^2 \equiv \left(\frac{\partial U}{\partial z}\right)^2 + \left(\frac{\partial V}{\partial z}\right)^2$$

and, for Eqs. (16a)–(16f), we have

$$D = 1 + d_1 G_M + d_2 G_H + d_3 G_M G_H + d_4 G_H^2 +$$

$$+\left[d_5 G_H^2 - d_6 G_M G_H\right]G_H, \qquad (16h)$$

$$d_1 = \frac{2}{3}\alpha_2^2,\ d_2 = \frac{10}{3}\frac{\alpha_3}{c_{1\theta}},\ d_3 = \frac{2}{3}\alpha_2\frac{\alpha_3}{c_{1\theta}}(\alpha_2-\alpha_5),$$

$$d_4 = \frac{11}{3}\left(\frac{\alpha_3}{c_{1\theta}}\right)^2,\ d_5 = \frac{4}{3}\left(\frac{\alpha_3}{c_{1\theta}}\right)^3,\ d_6 = \frac{2}{3}\alpha_2\alpha_5\left(\frac{\alpha_3}{c_{1\theta}}\right)^2,$$

$$s_0 = \frac{2}{3}\alpha_2,\ s_1 = \frac{1}{\alpha_2}\left(\frac{\alpha_3}{c_{1\theta}}\right),\ s_2 = \alpha_2 - \alpha_5,$$

$$s_3 = \alpha_5\left(\frac{\alpha_3}{c_{1\theta}}\right),\ s_4 = \alpha_3\alpha_5,\ s_5 = \alpha_5 + \frac{4}{3}\alpha_2,\ s_6 = \frac{\alpha_3}{c_{1\theta}},$$

$$\alpha_5 = \frac{1-C_{2\theta}}{C_{1\theta}}. \qquad (16i)$$

The variance of the vertical turbulent velocity and the horizontal heat fluxes are determined from the expressions

$$\left\langle w^2\right\rangle = \frac{1}{D}\{\frac{2}{3}E(1+s_6 G_H) + \frac{4}{3}\alpha_3\alpha_5(\tau\beta g)^2\left\langle\theta^2\right\rangle\times$$

$$\left(1-\frac{1}{2}\alpha_2\alpha_5 G_M + s_6 G_H\right)\}, \qquad (16j)$$

$$\left\langle u\theta\right\rangle = \frac{1}{D}\{\frac{2}{3}E\tau\frac{1}{c_{1\theta}}[\alpha_2 + (\alpha_2+\alpha_5)s_6 G_H +$$

$$+\alpha_5]\tau\frac{\partial U}{\partial z}\}\frac{\partial\Theta}{\partial z} -$$

$$-\frac{1}{D}\tau\frac{\partial U}{\partial z}\alpha_5(\tau\beta g)\left\langle\theta^2\right\rangle\left\{\alpha_5\left(1+\frac{2}{3}\alpha_2^2 G_M\right)+\right.$$

$$\left.\left(\alpha_5 - \frac{4}{3}\alpha_2\right)s_6 G_H +\right.$$

$$\left.+\frac{2}{3}s_6\alpha_2^2\alpha_3 G_M G_H - \frac{4}{3}s_6^2\alpha_2 G_H^2\right\}, \qquad (16k)$$

$$\left\langle v\theta\right\rangle = \frac{1}{D}\{\frac{2}{3}E\tau\frac{1}{c_{1\theta}}[\alpha_2 + (\alpha_2+\alpha_5)s_6 G_H +$$

$$\alpha_5]\tau\frac{\partial V}{\partial z}\}\frac{\partial\Theta}{\partial z} - \frac{1}{D}\tau\frac{\partial V}{\partial z}\alpha_5(\tau\beta g)\left\langle\theta^2\right\rangle\times$$

$$\{\alpha_5(1+\frac{2}{3}\alpha_2^2 G_M) + (\alpha_5 - \frac{4}{3}\alpha_2)s_6 G_H +$$

$$+\frac{2}{3}s_6\alpha_2^2\alpha_3 G_M G_H - \frac{4}{3}s_6^2\alpha_2 G_H^2\}. \qquad (16l)$$

8.3. Constants of the Three-Parameter Model of Turbulence

For the correlations with pressure fluctuations of the dynamic turbulent field, the 'standard' models are used (Launder et al., 1975; Launder, 1996). These models were successfully applied in solving different problems; therefore, the values of the numerical coefficients in the model expressions for these correlations have been approved sufficiently well. These coefficients are presented (Launder, 1996) as the graphical dependence

$$(1 - c_2)/c_1 = 0{,}23. \qquad (16m)$$

For the relaxation coefficient in the model of the slow part of pressure-strain correlation $\Pi_{ij}^{(1)}$ (7b), the value: c_1 = 2.0 is taken from the commonly used range between 1.5 and 2.0. For c_1 = 2.0, the numerical value of the coefficient c_2 found from (16m) is 0.54. When selecting the value of the coefficient c_3 in the buoyancy terms $\alpha_3 B_{ij}$ in (7b), one can use the solution of simple problems with allowance for buoyancy effects (Gibson and Launder, 1978; Lumley and Monsfield, 1984), c_3 = 0.776. Here, for this coefficient, the value 0.8 is taken, which corresponds to the value obtained by Cheng et al. (2002) via the renormalization-group technique. Numerical values of the coefficients in the pressure-temperature correlation Π_i^{θ} in (7c) are $c_{1\theta}$ =3.28 and $c_{2\theta} = c_{3\theta}$ =0.5. These values are calibrated during modeling of different turbulent

stratified flows, both homogeneous and inhomogeneous (Kurbatskii, 2001; Sommer and So, 1995). We note that the numerical value coefficient c_1 calculated by Cheng et al. (2002) with use of the renormalization-group technique turned out to be 2.5. At the same time, it should be remembered that, for example, for the widely used $E-\varepsilon$ model of turbulence, this technique yields the values of the constants appearing in the ε - equation that are noticeably different from the values calibrated with the database of measurements and commonly used in computations. Numerical coefficients in the diffusion terms have the following values: σ_E =1.2, σ_ε =1.2, and σ_θ =0.6. In Eq. (5a) for the TKE dissipation rate, we have ψ_0 =3.8, $\psi_1 = \psi_2$ =2.4, and ψ_3 =0.3 (Andren, 1990).

Note that the improved three-parameter anisotropic model for the turbulent ABL includes eight base constants ($c_1, c_2, c_3, c_{1\theta}, c_{2\theta} = c_{3\theta}, \psi_0, \psi_1 = \psi_2, \psi_3$) and three Prandtl numbers ($\sigma_E, \sigma_\varepsilon, \sigma_\theta$), which enter into the models of processes of turbulent diffusion of the transfer equations for the functions E, ε, and $\langle\theta^2\rangle$. The calibrated numerical values of these constants remain invariant during the solution of any problems of atmospheric turbulent flows with calculation of not only the distributions of average hydrothermodynamic fields but also the distributions of anisotropic turbulent momentum fluxes (normal and tangential turbulent stresses) and components of the vector of turbulent heat flux. The invariance of numerical values for the set of constants is a natural requirement that must be satisfied in any model that is constructed on the basis of the RANS (Reynolds Average Navier–Stokes) approximation and that claims to obtain results consistent with the data of measurements and observations for a wide class of problems of stratified atmospheric flows.

8.4. *Calculation of the Effects of Urban Roughness on a Flow in the ABL*

In this numerical test, the urban heat island is modeled through specification of the temperature difference between the urbanized surface and its vicinities and the time-dependent boundary condition for the temperature models a 24-h cycle of heating the Earth's surface by the Sun. For this reason, the mechanical factors are implemented by the parameterization scheme completely, whereas the contribution to the balance of potential temperature is implemented only approximately (heating/cooling of the surfaces of buildings). The urban roughness effects are calculated according to the scheme of Martilli et al. (2002).

8.5. *Boundary Conditions for System of Equations of the ABL (14a)–(14e)*

Following by Yamada and Mellor (1975)], one can find an expression for the ratio of the horizontal wind speeds at the first two computational nodes above the surface ($z_2 > z_1 > 0$). This expression represents the finite-difference boundary condition for the wind speed at the lower boundary and is written as

$$\frac{U_1}{U_2} = \frac{V_1}{V_2} = \frac{ln(z_1/z_0)}{ln(z_2/z_0)}. \qquad (18a)$$

In our numerical test, the temperature measured at the ground surface is interpolated with dependence (11a). Therefore, according to Yamada and Mellor (1975), the boundary condition in a finite-difference form is also used for the temperature:

$$\hat{\Theta}_2 = \Delta_\theta \hat{\Theta}_3 + \hat{\Theta}_g(1-\Delta_\theta),\ \Delta_\theta = \frac{\ln z_2/z_{0t}}{\ln z_3/z_{0t}}, \qquad (18b)$$

where z_{0t} = 0.6z_0 (z_0 = 0.1 m in calculations).

In order to calculate turbulent fluxes near the surface, the MOST is used to relate vertical gradients in the surface layer and the empirical function Φ, obtained from the data of the Kansas experiment, is taken from Andre et al. (1978). The boundary conditions are specified at the first (from the surface) computational node and have the form

$$E_1 = u_{*0}^2/\sqrt{c_\mu}, \qquad (18c)$$

$$\varepsilon_1 = u_{*0}^3(\Phi/0,41z_1 - 1/0,41L), \qquad (18d)$$

$$\langle\theta^2\rangle = \theta_{*0}^2 \begin{cases} 4(1-8,3\zeta)^{-2/3}, & \zeta \le 0 \\ 4, & \zeta > 0 \end{cases}, \qquad (18e)$$

$$\theta_{*0} = \frac{k}{\mathrm{Pr}_t}\left[\hat{\Theta}(z_1) - \hat{\Theta}_g\right] \times \left[\ln(z_1 + z_{0t})/z_0 + \ln(z_0/z_{ot}) - \Phi\right]^{-1}, \qquad (18f)$$

$$\Phi = \begin{cases} (1-15\zeta)^{-1/4}, & \zeta \le 0 \\ 1+5\zeta, & \zeta > 0 \end{cases}$$

$$\zeta = z/L,\ L = u_{*0}^2/(0,41\beta g\theta_{*0}). \qquad (18g)$$

The frictional velocity u_{*0} and frictional temperature θ_{*0} are computed using MOST and the no iterative scheme of Louis (1979).

Acknowledgments

This study was supported by the Russian Foundation for Basic Research (project No. 06-05-64002).

8.6 ***References***

Andre, J. C., De Moor, G., Lacarrere, P., Therry, G. and du Vachat, R. 1978: Modeling the 24-hour Evolution of the Mean and Turbulent Structures of the Planetary Boundary Layer. *J. Atmos. Sci*. **35**, 1861–1883.

Andren, A. 1990: Evaluation of a Turbulence Closure Scheme for Air-Pollution Applications. *J. Appl. Meteor.* **29**, 224–239.

—. 1990. A TKE-Dissipation Model for the Atmospheric Boundary Layer. *Bound.-Layer Meteor*. **56**, 207–221.

Bornstein, R. and Johnson, D. S. 1977: Urban-Rural Wind Velocity Differences. *Atmos. Environ.* **11**, 597–604.

Cheng, Y., Canuto, V. M. and Howard, A. M. 2002: An Improved Model for the Turbulent PBL. *J. Atmos. Sci.* **59**, 1500–1565.

Enger L. 1986: A higher order closure model applied to dispersion in a convective PBL. *Atmos. Environ.* **20**, 879-894.

Feigenwinter, C. 1999: *The Vertical Structure of Turbulence above an Urban Canopy*. PhD Thesis. University of Basel, 76 pp.

Fernando, H. J. S., Lee, S. M., Anderson, J., Princevac, M., Pardyak, E. and Grossman-Clarke, S. 2001: Urban Fluid Mechanics: Air Circulation and Contaminant Dispersion in Cites, *Environmental Fluid Mech*. **1**, 107–164.

Gibson, M. M. and Launder, B. E. 1978: Ground Effects on Pressure Fluctuation in the Atmospheric Boundary Layer. *J. Fluid Mech*. **86**, 491–511.

Girimaji, S. S. and Balachandar, S. 1998: Analysis and Modeling of Buoyancy-Generated Turbulence Using Numerical Data. *Int. J. Heat Mass Transfer* **41**, 915–929.

Kolmogorov, A. N. 1942: Equations of Turbulent Motion of an Incompressible Fluid. *Izv. Akad. Nauk SSSR*, *Ser. Fizicheskaya* **6** (1–2), 56–58.

Kurbatskii, A. F. and Kazakov, A. V. 1999: Explicit Algebraic Model of Turbulent Heat Transfer for a Developed Flow in a Rotating Round Pipe. *Thermophysics and Aeromechanics*. **6**, 231–240.

—, 2001: Computational Modeling of the Turbulent Penetrative Convection above the Urban Heat Island in a Stably Stratified Environment. *J. Appl. Meteor*. **40**, 1748–1761.

—, and Kurbatskaya, L. I. 2001: Penetrative Turbulent Convection over a Heat Island in a Stably Stratified Environment. *Izv. Akad. Nauk, Fiz. Atm. Okeana* **37**, 149–161 [*Izv., Atmos. Ocean. Phys.* **37**, 135– 146.

—, Kurbatskii, A. F 2005: Numerical Investigation of Surface Heat Spot Effect on Atmospheric Bound ary Layer Structure. *Thermophysics and Aeromechanics*. **12**, 39–58.

Launder, B. E. 1975: On the Effects of Gravitational Field on the Turbulent Transport of Heat and Momentum. *J. Fluid Mech.* **67**, 569–581.

—, Reece, G. and Rodi, W. 1975: Progress in the Development of a Reynolds-Stress Turbulent Closure. J. Fluid Mech. **68**, 537–566.

—, 1996. An Introduction to Single-Point Closure Methodology. In: *Simulation and Modeling of Turbulent Flows*. Oxford Univ. Press, New York, pp. 243-310.

Louis, J. F. 1979: A parametric model of vertical eddy fluxes in the atmosphere. *Bound.-Layer Meteor.* **17**, 187-202.

Louka, P., Belcher, S. E. and Harrison, R. G. 2000: Coupling between Air Flow in Streets and the Well Developed Boundary Layer Aloft. *Atmos. Environ*. **34,** 2613–2621.

Lu, L., Araya, S. P., Snyder, W. H. and Lawson, R. E. 1997: A laboratory study of the heat island in a calm stably stratified environment. Pts. I and II. *J. Appl. Meteor.* **36**, 1377-1402.

Lumley, J. L. and Monsfield, P. 1984: Second Order Modeling of Turbulent Transport in the Surface Mixed Layer. *Bound.-Layer Meteor*. **30**, 109–142.

Martilli, A., Clappier, A., Rotach, M. W. 2002: An Urban Exchange Parameterization for Mesoscale Models. *Bound.-Layer Meteor.* **104**, 261–304.

Mellor, G. L. and Yamada, T.: 1974: A Hierarchy of Turbulence Closure Models for Planetary Boundary Layer, *J. Atmos. Sci*. **31**, 1791–1806.

—, 1982: Development of a Turbulence Closure Model for Geophysical Fluid Problems. *Rev. Geophys. Space Phys*. **20**, 851–875.

Moussiopoulos N., Sahm P., Karatzas K., Papalexiou S., Karagianndis. 1997: Assessing the impact of the new Athens airport to urban air quality with contemporary air pollution models. *Atmos. Environ.* **31**, 1497-1511.

Oikawa, S. and Meng, Y. 1995: Turbulence Characteristics and Organized Motion in a Suburban Roughness Sublayer. *Bound.-Layer Meteor*. **74**, 289–312.

Raupach, M. R., Antonia, R. A. and Rajagoplan, S. 1991: Rough-Wall Turbulent Boundary Layers, *Appl. Mech. Rev*. **44**, 79–90.

Roache, P. J. 1976. *Computational Fluid Dynamics*. Hermosa. Albuquerque, pp.615.

Rotach, M. W. 1991. Turbulence within and above an Urban Canopy. ETH Dissertation, 9439.

—, 1993a: Turbulence Closure to a Rough Urban Surface. Part I: Reynolds Stress. *Bound.-Layer Meteor*. **65**, 1–28.

—, 1993b: Turbulence Closure to a Rough Urban Surface. Part II. *Bound.-Layer Meteor*. **65**, 1–28.

—, 1995: Profiles of Turbulence Statistics in and

above an Urban Street Canyon. *Atmos. Environ*. **29**, 1473–1486.

—, 1999: On influence of the urban roughness sublayer on turbulence and dispersion. *Atmospheric Environment*. **33**, 4001-4008.

Roth, M. 2000: Review of Atmospheric Turbulence over Cites. *Q. J. Roy. Meteor. Soc*. **126**, 941–990.

Sommer, T. P. and So, R. M. C. 1995: On the Modeling of Homogeneous Turbulence in a Stably Stratified Flow. *Phys. Fluids* **7**, 2766–2777.

Spanton, A. M. and Williams, M. L. 1988: A Comparison of the Structure of the Atmospheric Boundary Layers in Central London and a Rural/Suburban Site Using Acoustic Sounding. *Atmos. Environ*. **22**, 211–223.

Uno, I. and Wakamatsu, S. 1992: Observed Structure of the Nocturnal Urban Boundary Layer and Its Evolution into a Convective Mixed Layer. *Atmos. Environ*. **B 26**, 45– 57.

Vu, T. C., Ashie, Y. and Asaeda, T. 2002: A Turbulence Closure Model for the Atmospheric Boundary Layer Including Urban Canopy. *Bound.-Layer Meteor.* **102**, 459– 490.

Yamada, T. and Mellor, G. 1975: A Simulation of the Wangara Atmospheric Boundary Layer Data. *J. Atmos. Sci.,* **32**, 2309-2329.

Zeman, O. and Lumley, J. L. 1979: Buoyancy Effects in Entraining Turbulent Boundary Layers: A Second-Order Closure Study. In: *Turbulent Shear Flows*, Springer, Berlin, **1**, pp. 295– 302.